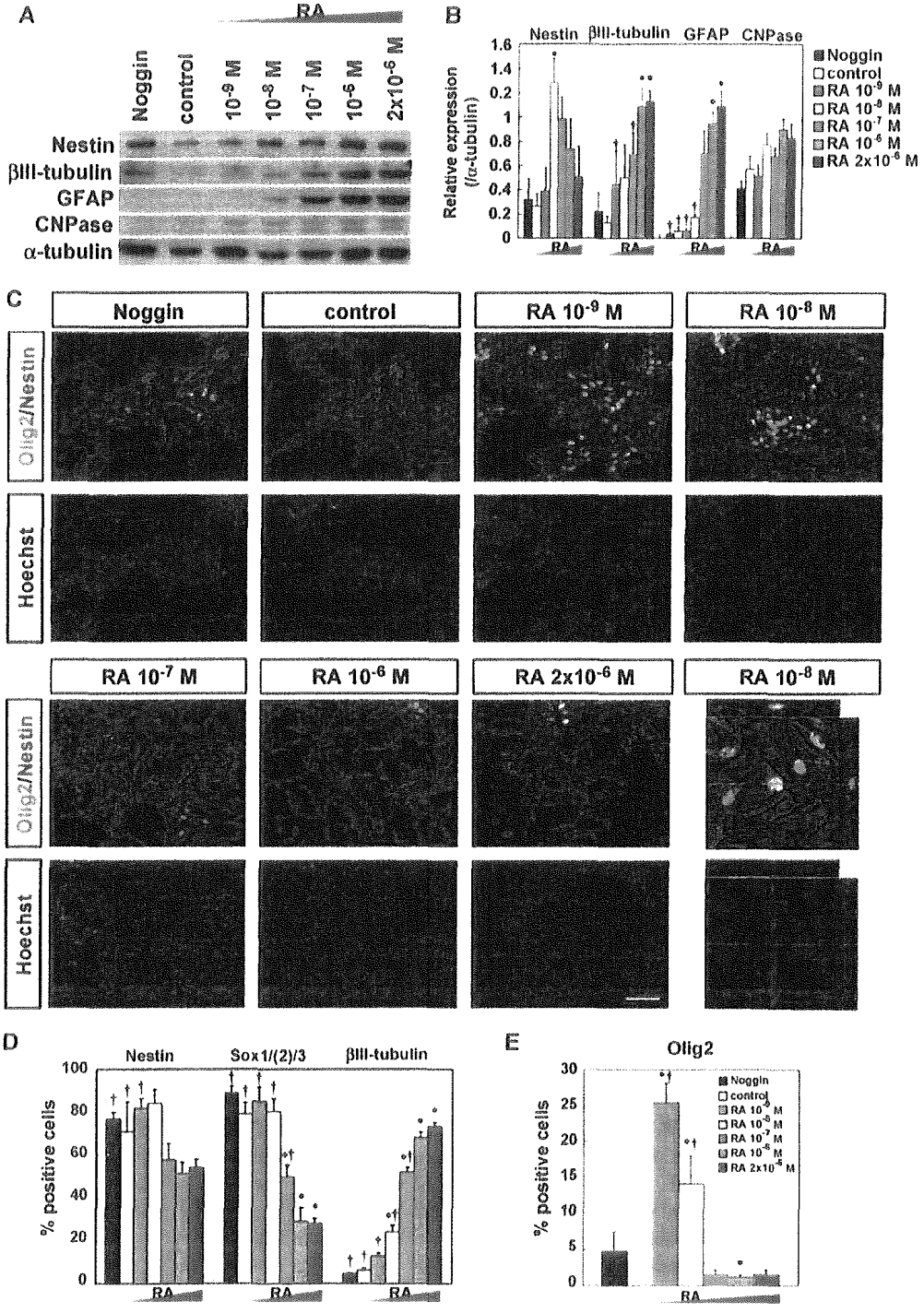

Fig. 3. RA promotes neural differentiation in a concentration-dependent manner and regulates the differentiation of ES-cell-derived neural progenitors. (A) Western blot analysis of markers for neural differentiation in EBs cultured for 6 days. (B) Quantitative analysis was performed with Scion Image. The amounts of proteins were normalized to those of α-tubulin ($n = 3$, mean ± SEM, *, $P < 0.05$ vs. control, †, $P < 0.05$ vs. RA 2×10^{-6} M). (C) Immunocytochemistry of dissociated EBs for Olig2 and Nestin. Nuclear localization of Olig2 in Nestin immunoreactive cells was confirmed by three-dimensional reconstruction of confocal microscopic images (right end of lower panels). (D, E) The proportions of cells positive for Nestin, Group B1 Sox, Olig2, and βIII-tubulin among the total number of cells in dissociated EBs were determined by immunocytochemically. Immunoreactive cells as a percentage of the total number of cells counted on the basis of nuclear staining with hoechst33342 are shown ($n = 3$, mean ± SEM, *, $P < 0.05$ vs. control, †, $P < 0.05$ vs. RA 2×10^{-6} M). The percentages of cells expressing Olig2, Group B1 Sox, and Nestin were higher in dissociates of EBs treated with low-RA ($<10^{-8}$ M) than in EBs treated with high-RA ($>10^{-7}$ M). Scale bar: 50 μm.

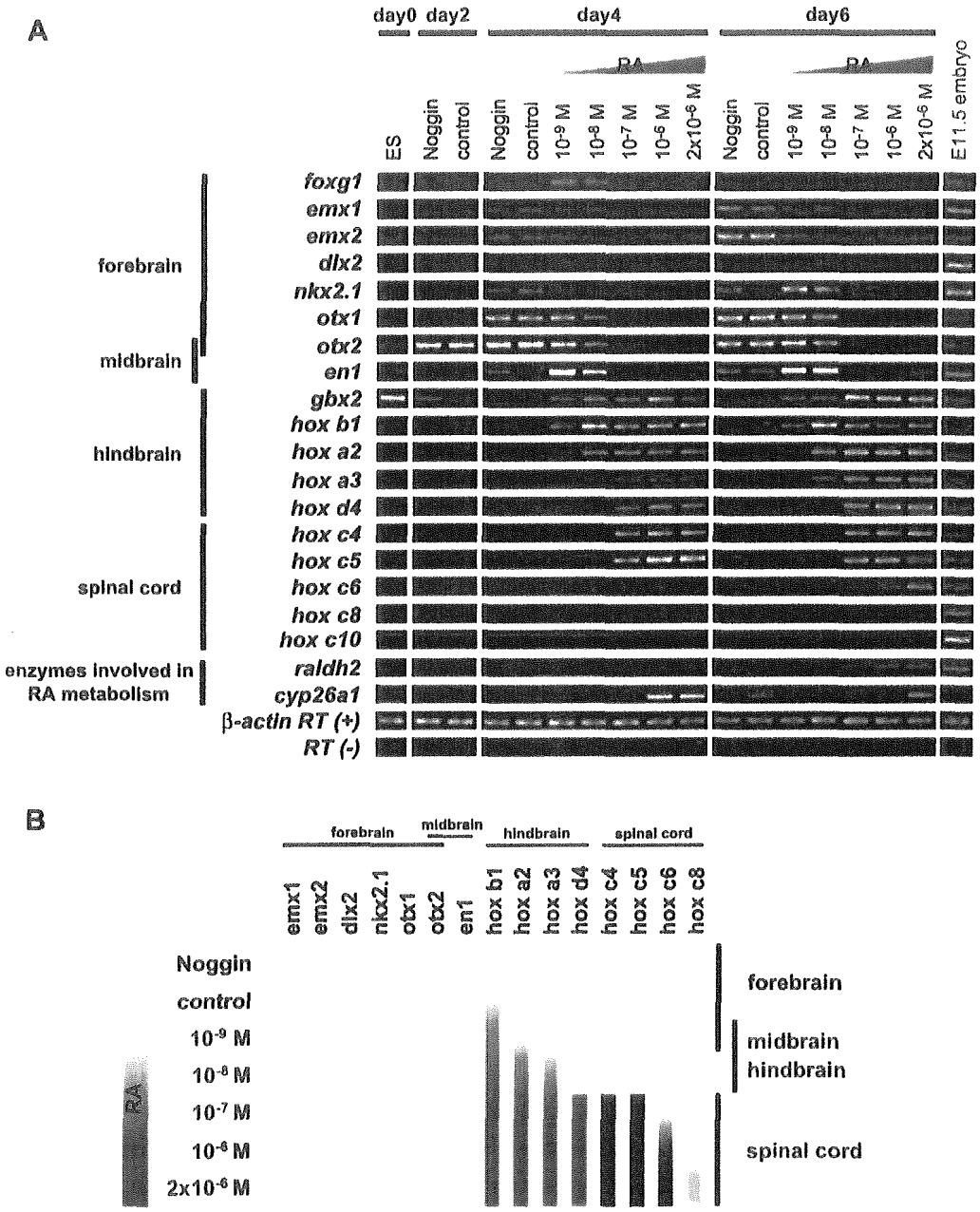

Fig. 4. Concentration-dependent effects of RA on the specification of rostrol-caudal positional identity of ES-cell-derived neural progenitors. (A) Effect of RA on rostrol-caudal axis formations was analyzed by RT-PCR on days 0, 2, 4, and 6 of differentiation. The expression patterns are summarized in (B). RA caudalized ES-cell-derived neural cells in a concentration-dependent manner. Control and Noggin-treated-EBs expressed forebrain-type markers, whereas EBs treated with low-RA and high-RA expressed midbrain–hindbrain-type markers and spinal-cord-type markers, respectively.

Fig. 5. RA caudalizes EB-derived neurons in a concentration-dependent manner. (A) Immunocytochemical analysis of neural progenitors and neurons differentiated from dissociated EBs with Otx1, which is expressed in developing forebrain and midbrain, and Phox2B, Lim3, HB9, and Isl-1/2, which are expressed in developing motor neurons and their progenitors. Immunoreactive cells as a percentage of the total number of cells counted on the basis of the nuclear staining with hoechst33342 are shown in B ($n = 3$, mean ± SEM, *, $P < 0.05$ vs. control, †, $P < 0.05$ vs. RA 2×10^{-6} M). (C) RT-PCR analysis of *phox2b* and *hb9*. Control and Noggin-treated EBs generated significant numbers of Otx1-and Group B1 Sox-positive anterior neural progenitors. Low-RA (10^{-9}–10^{-8} M) induced many Phox2b-positive hindbrain brachial and visceral motor neurons and fewer Otx1/Group B1 Sox-positive anterior neural progenitors, whereas high-RA (>10^{-7} M) induced more HB9-positive hindbrain and spinal cord somatic motor neurons without any Otx1-positive cells. Scale bar: 50 μm.

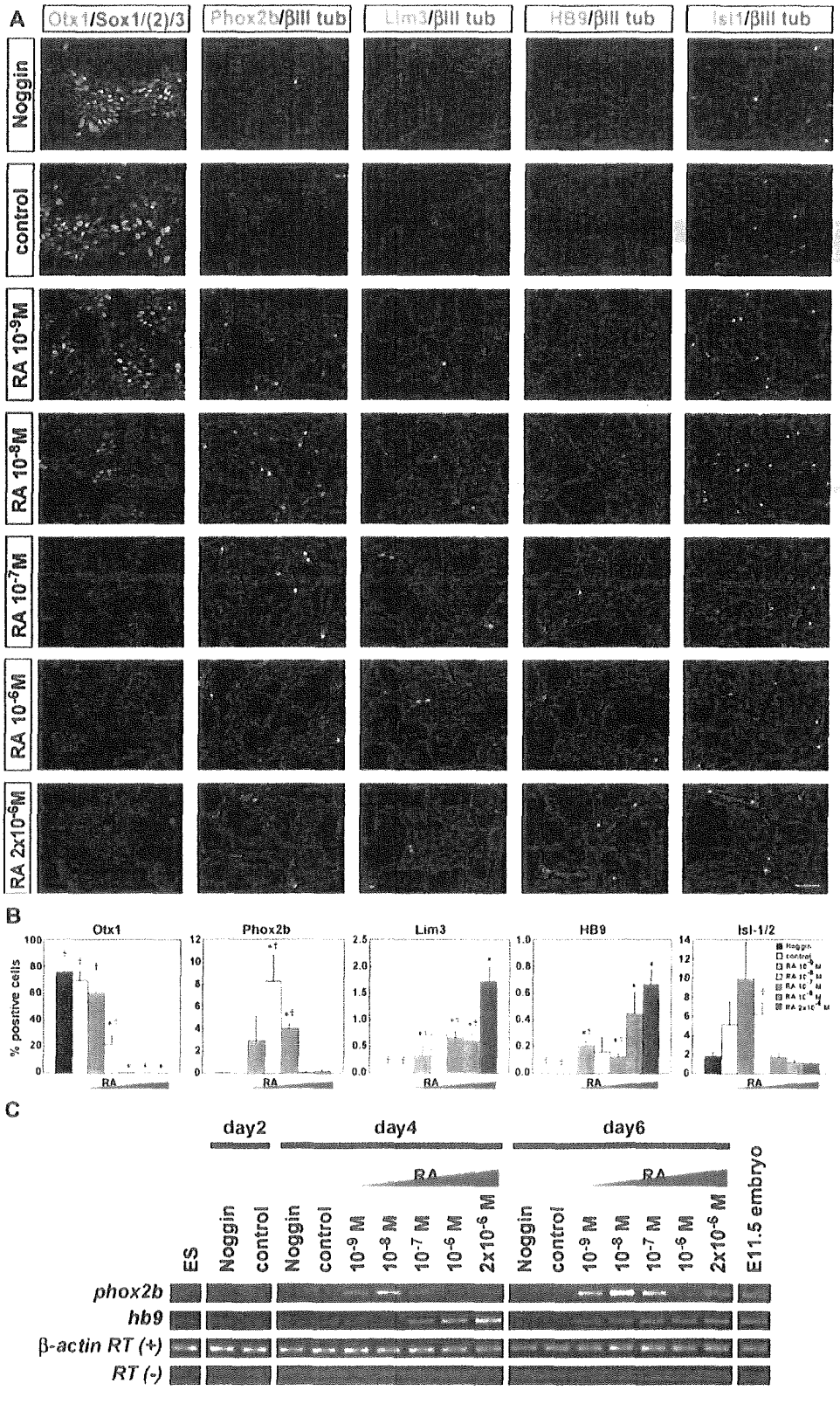
A
Otx1/Sox1/(2)/3
Phox2b/βIII tub
Lim3/βIII tub
HB9/βIII tub
Isl1/βIII tub
Noggin
control
RA 10-9M
RA 10-8M
RA 10-7M
RA 10-6M
RA 2x10-6M
B
Otx1
Phox2b
Lim3
HB9
Isl-1/2
% positive cells
RA
C
day2
day4
day6
RA
ES
Noggin
control
10-9 M
10-8 M
10-7 M
10-6 M
2x10-6 M
E11.5 embryo
phox2b
hb9
β-actin RT (+)
RT (-)

Niederreither et al., 2000; Schuurmans and Guillemot, 2002; Wurst and Bally-Cuif, 2001). As shown in Fig. 4, EBs were caudalized in a concentration-dependent manner during the first 2 days of RA exposure (days 2–4). After day 4, control and Noggin-exposed EBs expressed genes specific to forebrain (*emx1*, *emx2*, *nkx2.1*, *otx1*, *otx2*) and midbrain–hindbrain (*otx1*, *otx2*, *en1*), but no hindbrain or spinal cord markers. EBs treated with low-RA mainly expressed midbrain–hindbrain markers (*otx1*, *otx2*, *en1*, *gbx2*, *hoxb1*, *hoxa2*, *hoxa3*), and did not express spinal cord markers (*hoxc4*, *hoxc5*, *hoxc6*, *hoxc8*, *hoxc10*). Expression of telencephalic markers (*emx1*, *emx2*, *dlx2*) in EBs treated with low-RA was lower than in control and Noggin-exposed EBs. However, at day 4, expression of one of the telencephalic markers, *foxg1*, was somehow highest in the EBs exposed to low-RA. On the other hand, high-RA induced expression of hindbrain and rostral spinal cord markers (*hoxc4*, *hoxc5*, *hoxc6*) and reduced expression of forebrain and midbrain markers. These patterns of gene expression were detected at day 4 and were maintained thereafter. The expression levels of enzymes involved in RA metabolism, *raldh2* and *cyp26a1* (Fig. 4A), were higher in EBs treated with high-RA, a finding that was consistent with the EBs exposed to high-RA acquiring the identity of rostral spinal cord, where the concentration of RA and the expression level of its synthesizing enzyme Raldh2 are the highest in the developing CNS (Swindell et al., 1999). The RA catabolizing enzyme Cyp26a1 may have been induced by high-RA as part of a negative feedback mechanism. The total gene expression patterns indicating rostro-caudal specification in EBs differentiated under different conditions are summarized in Fig. 4B. The concentration-dependent caudalization of EBs by RA treatment shown by the result of the RT-PCR analysis was confirmed by immunocytochemistry of dissociated EBs with antibodies for markers expressed in developing forebrain and midbrain (Otx1) (Acampora et al., 1998), visceral or brachial motor neurons in the hindbrain (Phox2b) (Pattyn et al., 2000), and somatic spinal motor neurons (HB9, Lim3) (Arber et al., 1999) (Figs. 5A,B). Virtually all of the marker-positive cells were also positive for either a neural progenitor marker Group B1 Sox, or pan-neuronal marker βIII-tubulin. A significant number of cells derived from EBs and grown under all conditions expressed Isl-1/2, a marker of postmitotic cholinergic neurons, including not only spinal motor neurons but those in ventral forebrain (Kohtz et al., 2001; Wang and Liu, 2001). Somatic motor neurons of the hindbrain and spinal cord expressing Lim3 and HB9 were found more frequently when treated with high-RA, whereas hindbrain visceral or brachial motor neurons expressing Phox2b were found more frequently when treated with low-RA. By contrast, an enormous number of neural progenitors that were positive for both Otx1 and Group B1 Sox and acquired anterior positional identity were induced from control and Noggin-treated EBs, and less frequently from low-RA treated EBs, whereas no such cells were induced from high-RA-treated EBs. Taken together, these findings indicate that RA induced both caudalization of EBs based on the expression patterns of regionally specific genes during neural induction and neuronal differentiation in a concentration-dependent manner, resulting in significant generation of forebrain and midbrain (control and Noggin), hindbrain (low-RA), and spinal cord (high-RA) types of neural progenitors or neurons, respectively.

RA controls dorso-ventral axis formation

To determine the effect of RA on dorso-ventral axis specification of EB-derived cells, we investigated the expression of class I genes (*pax7*, *dbx1*, *dbx2*, *irx3*, *pax6*, whose expression is *repressed* by Shh in early CNS development) and class II genes (*nkx6.2*, *nkx6.1*, *olig2*, *nkx2.2*, whose expression is *activated* by Shh). These genes are differentially expressed along the dorso-ventral axis in the progenitor domains of developing hindbrain and spinal cord (Jessell, 2000). As shown in Fig. 6, EBs treated with low-RA expressed both class I and class II genes, indicating that they were composed of various populations that had acquired their identities throughout the dorsal to ventral neural tube. Interestingly, on the other hand, treatment with high-RA raised the expression levels of class I genes and significantly reduced those of class II genes except *olig2* at day 4, in comparison to treatment with low-RA. Thus, high-RA caused dorsalization of neural progenitor cells in EBs. To investigate the mechanism underlying the action of RA in specifying dorso-ventral identity, we investigated its effects on expression of the N-terminus of Shh protein (Shh-N) and *sonic hedgehog* (*shh*) mRNA. Mouse Shh is produced as a 49-kDa secreted protein that post-translationally cleaves to yield two mature proteins: an approximately 19-kDa N-terminal fragment that contains the signaling portion of the molecule and an approximately 27-kDa C-terminal fragment, which has auto-processing activity (Marti et al., 1995; Porter et al., 1995, 1996; Roelink et al., 1995). We found that expression of both the Shh-N protein and *shh* mRNA was significantly up-regulated by exposure to low-RA in day 4–6 EBs (Figs. 7A–C), but that further increasing the RA concentration ($>10^{-7}$ M) induced their down-regulation instead. More specifically, the RA-responsive increase in Shh-N expression appeared to be concentration-dependent up to 10^{-8} M, but was completely abrogated at 10^{-7} M and higher concentrations. On the other hand, the peak level of full-length Shh protein expressed in response to exposure to 10^{-8} M of RA was maintained even in EBs exposed to higher concentrations of RA. These results suggested that the ventralization of neural progenitors in EBs exposed to low-RA might be caused by an enhanced expression of Shh-N. However, we

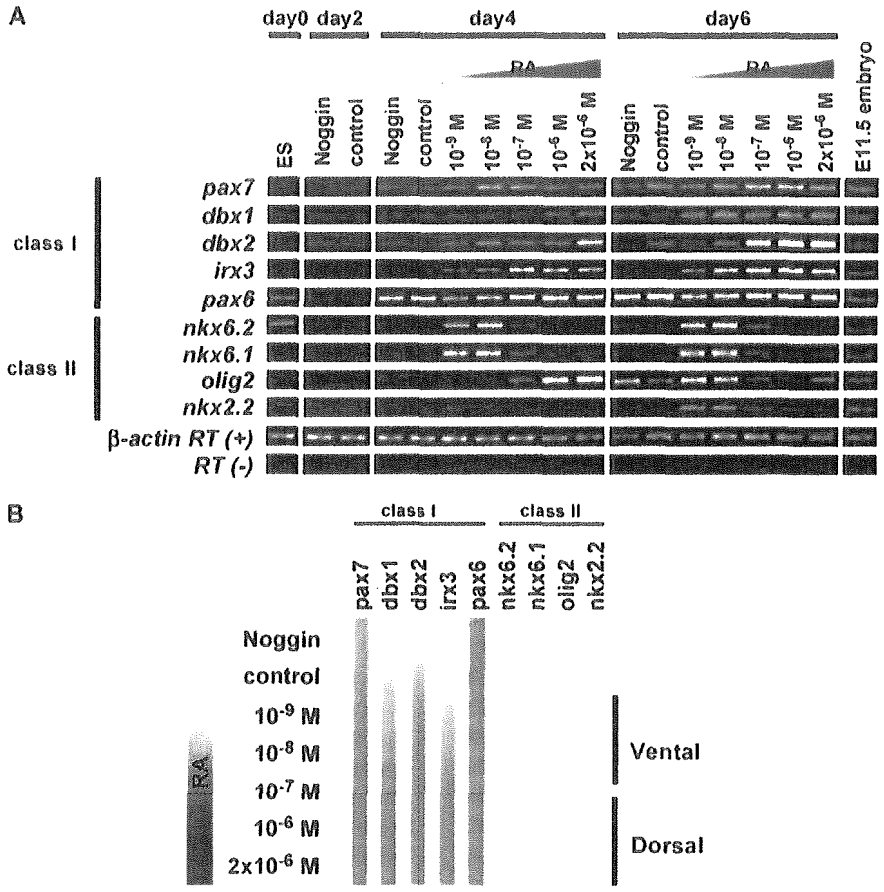

Fig. 6. Specification of the dorso-ventral identity of ES-cell-derived neural progenitors is regulated by RA. (A) RT-PCR analysis of class I and class II genes, which define dorsol-ventral positional identity. The expression patterns are summarized in (B). EBs treated with low-RA (10^{-9}–10^{-8} M) expressed both class I and II genes (class II > class I), which indicated that both ventral and dorsal neural progenitors had been induced, whereas EBs treated with high-RA (>10^{-6} M) expressed only class I gene, indicating dorsal neural progenitors had been induced.

could not rule out the possibility of the opposite causal relationship; that is, that low-RA induced enhanced expression of Shh-N protein and the expression of *shh* mRNA resulted from the ventralization of EB-derived cells that had been induced by low-RA treatment through an unknown mechanism. To address this issue, we treated EBs exposed to RA with recombinant Shh-N protein and cyclopamine, an inhibitor of Shh signaling (Chen et al., 2002a,b; Incardona et al., 1998). In the absence of cyclopamine treatment, EBs exposed to low-RA expressed both class I (*pax7*, *dbx1*, *dbx2*, *irx3*, and *pax6*) and class II genes (*nkx6.2*, *nkx6.1*, *olig2*, and *nkx2.2*), thereby indicating both dorsal and ventral phenotype. Treatment with 1 μM cyclopamine strongly down-regulated the ventral class II genes (*nkx6.2*, *nkx6.1*, *olig2*, and *nkx2.2*) and some of the class I genes (*dbx1* and *dbx2*), indicating a dorsalized phenotype (Figs. 7D,E). In addition, exposure to 50 nM of recombinant Shh-N protein enhanced expression of class II genes (*nkx6.2*, *nkx6.1*, *olig2*, and *nkx2.2*) but reduced *pax7* expression. These effects were abrogated by treatment with 1 μM cyclopamine (Figs. 7D,E). EBs treated with high-RA expressed higher levels of class I genes (*pax7*, *dbx1*, and *dbx2*, *irx3*, *pax6*), but lower levels of class II genes (*nkx6.2*, *nkx6.1*, *olig2*, and *nkx2.2*), thereby indicating a more dorsal phenotype than after low-RA treatment. However, high-RA treated EBs were ventralized by treatment with exogenous Shh-N, as shown by the up-regulation of class II genes (*nkx6.2*, *nkx6.1*, *olig2*, and *nkx2.2*) and down-regulation of *pax7*, and these changes were also abrogated by 1 μM cyclopamine treatment (Figs. 7D,E).

This alteration of dorso-ventral identity by RA, Shh-N, and cyclopamine was confirmed by the immunostaining of dissociated EBs with antibodies against Pax7, Nkx6.1, and Nkx2.2 (Fig. 8). Virtually all the marker-positive cells also stained with the antibodies against Group B1 Sox or Nestin, indicating they are neural progenitor cells. It was noteworthy that Shh-N treatment could induce only Nkx6.1-positive but not Nkx2.2-positive neural progenitors in EBs treated with high-RA, indicating that the ventralmost neural progenitors could not be efficiently derived under such conditions, but that they were capable of increasing the

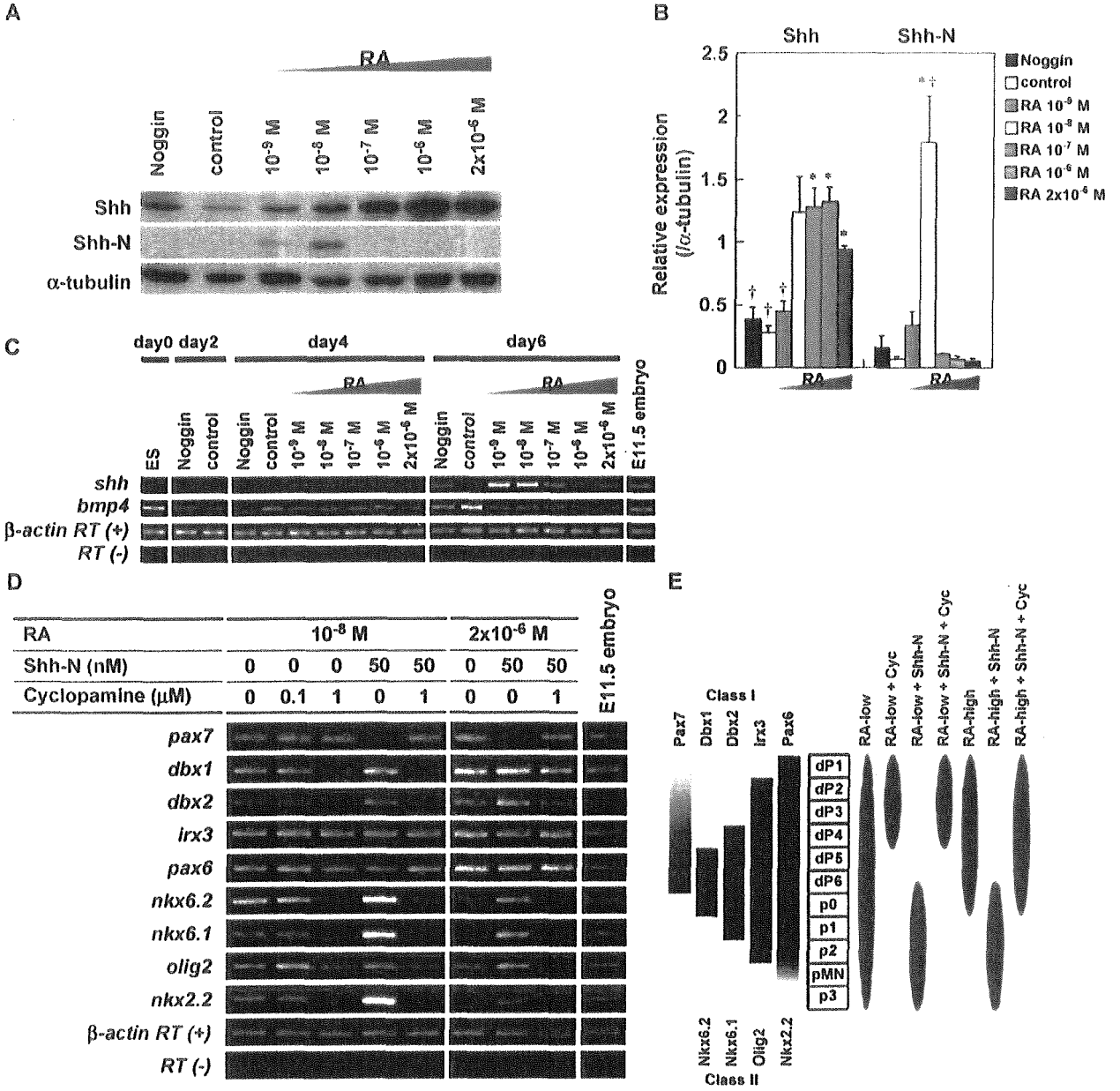

Fig. 7. Shh-N mediates RA-dependent dorso-ventral specification of ES-cell-derived neural progenitors. (A) Expression of Shh and its active N-terminal truncated form, Shh-N, in EBs cultured for 6 days, was analyzed by Western blotting. EBs were exposed to various concentrations of RA. Quantitative analysis was performed with Scion Image. The amounts of proteins were normalized to those of α-tubulin (B) ($n = 3$, mean ± SEM, *, $P < 0.05$ vs. control. †, $P < 0.05$ vs. RA 2×10^{-6} M). (C) RT-PCR analysis of *shh* and *bmp4*. Shh-N was more highly expressed in EBs treated with low-RA (10^{-9} M–10^{-8} M). (D) RT-PCR analysis of RA-exposed EBs treated with Shh-N and its inhibitor cyclopamine. Shh-N and cyclopamine were added together with RA on day 2. (E) Summary of expression patterns in vitro corresponding to in vivo. Cells from low-RA-treated EBs were a mixed population of dorsal-to-ventral neural progenitors and were capable of being dorsalized by inhibiting Shh signaling with cyclopamine. By contrast, exogenous Shh-N induced ventral neural progenitors were capable of being dorsalized by cyclopamine. Cells from high-RA-treated EBs showed dorsal positional identities. However, addition of Shh-N increased the number of ventral neural progenitors, and they were also capable of being dorsalized by cyclopamine treatment.

Fig. 8. Dorso-ventral specification of RA treated EBs is altered by Shh-N and cyclopamine. The alteration of dorso-ventral identity by RA, Shh-N, and cyclopamine was confirmed by the immunostaining of dissociated EBs with antibodies against Pax7 as a marker for dorsal neural progenitors, against Nkx6.1 as a marker for ventral neural progenitors, and against Nkx2.2 as a marker for ventralmost neural progenitors in combination with Group B1 Sox or Nestin as a marker for neural progenitors. Immunoreactive cells as a percentage of the total number of cells counted on the basis of the nuclear staining with hoechst33342 are shown in B ($n = 3$, mean ± SEM). Scale bar: 50 μm.

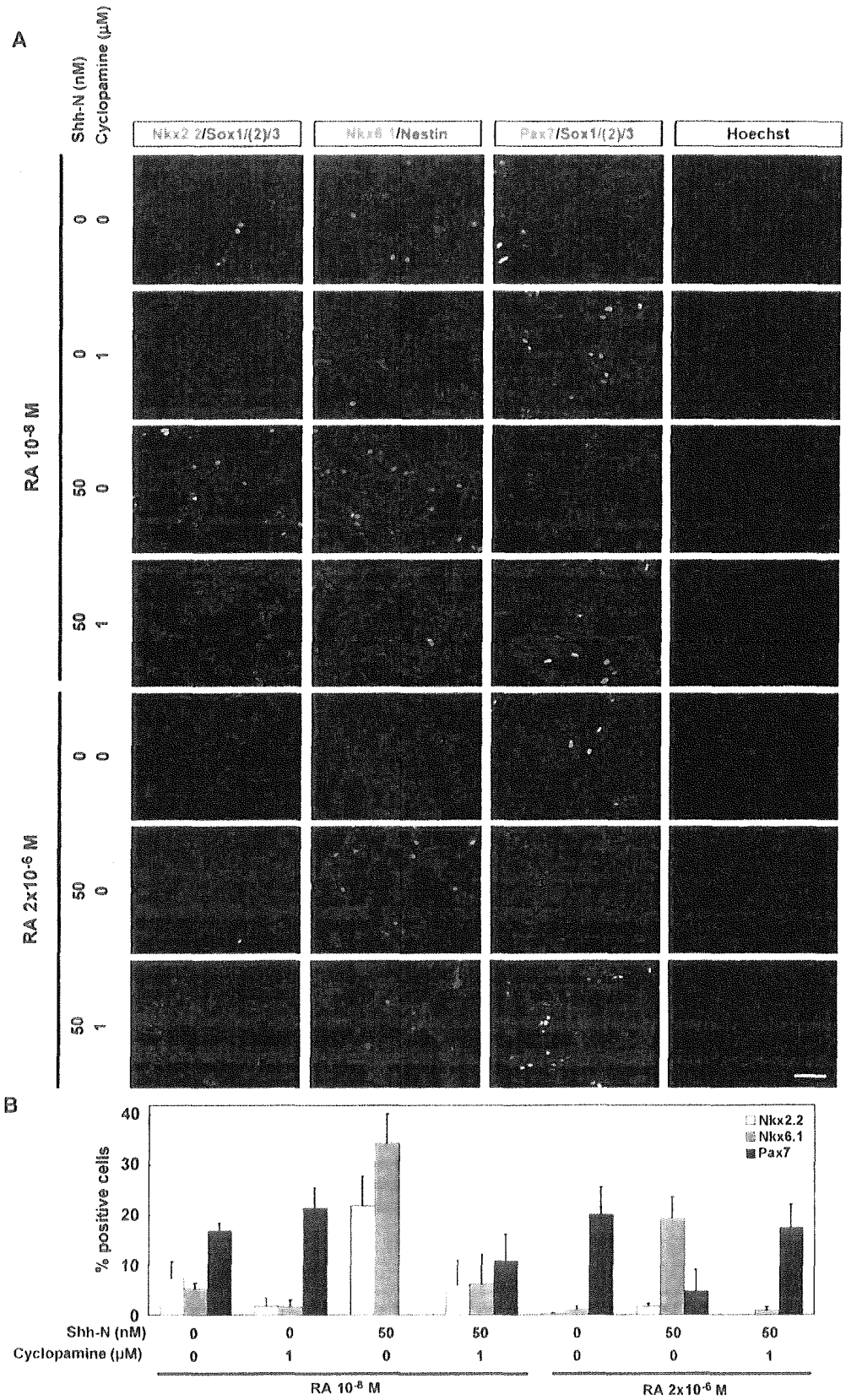
A
Shh-N (nM)
Cyclopamine (μM)
Nkx2.2/Sox1/(2)/3
Nkx6.1/Nestin
Pax7/Sox1/(2)/3
Hoechst
RA 10-8 M
RA 2x10-6 M
0
50
1
B
% positive cells
40
30
20
10
0
Nkx2.2
Nkx6.1
Pax7
Shh-N (nM)
Cyclopamine (μM)
RA 10-8 M
RA 2x10-6 M

number of Nkx6.1- or Nkx2.2-positive ventral neural progenitors in EBs treated with low-RA. The observation in EBs treated with high-RA is consistent with the previous report (Wichterle et al., 2002).

One of the major dorsalizing molecules in the CNS, *bmp4* (Caspary and Anderson, 2003; Jessell, 2000; Knecht and Bronner-Fraser, 2002), was not very strongly affected by RA, Shh-N, or cyclopamine, suggesting a lesser contribution of the BMP signal to this RA-mediated dorso-ventral specification (Fig. 7C, data not shown). These results indicate that differentiating EBs were ventralized by low-RA through induction of endogenous Shh-N protein, and that the effect was abrogated by cyclopamine and enhanced by the addition of exogenous Shh signal (Figs. 7D,E and 8).

Positional identity regulated by the RA concentration is mainly determined during the first 2 days of exposure to RA

According to the RT-PCR analysis of EBs cultured according to the 2−/4+ protocol, the expression patterns of most of the regionally specific markers were determined by day 4 and maintained unchanged thereafter. This observation raised two possibilities. One possibility is that the first 2 days of exposure to RA are critical to the determination of positional identity, and the second is that the effect of the RA concentration was altered during the later culture period by degradation of RA. To determine which of these possibilities was true, we performed a RT-PCR analysis of EBs cultured according to other protocols in which the times when RA is added or the duration of exposure to RA (2−/2+/2−, 2−/2+/2+, and 4−/4+ protocols) is different from the 2−/4+ protocol (Suppl. Fig. 1). Expression of *oct3/4* had been maintained before the addition of RA, but no expression of other markers except *otx2*, whose mRNA was expressed even in undifferentiated ES cells, had been detected in any of the culture protocols, including the 4−/4+ protocol. The expression patterns of most of regionally specific markers were determined by day 4 of the 2−/2+/2− and 2−/2+/2+ or by day 6 of the 4−/4+ protocol, and were virtually the same in all protocols as observed in the 2−/4+ protocol, and they were maintained thereafter as well (Suppl. Fig. 2). Overall, positional identity is determined during the first 2 days of exposure to RA and is maintained thereafter regardless of the presence or absence of RA in later culture periods.

Discussion

The pluripotent embryonic stem cell is a valuable in vitro model for studying the effects of various factors on cell lineage decisions in very early embryonic stages of mammalian development, and the effect of RA signaling on the differentiation of ES cells and neural induction, in particular, has been extensively studied. In addition to previous reports showing that RA promotes neural differentiation of ES cells and caudalization of the positional identity of their progeny (Bain et al., 1995, 1996; Fraichard et al., 1995; Gajovic et al., 1997; Renoncourt et al., 1998; Strubing et al., 1995; Wichterle et al., 2002), the results of the present study demonstrate the novel and precise actions of RA on neural differentiation and acquisition of positional identity by ES-cell-derived neural cells.

Effect of the concentration of RA on ES cell differentiation

It is well known that exposure of growing EBs to high-RA markedly increases the rate of neural differentiation, whereas low-RA induces more mesodermal cells (Rohwedel et al., 1999). Higher concentrations of RA also promote faster differentiation of ES cells, as indicated by the pattern of *oct3/4* expression, which was down-regulated more rapidly in EBs exposed to higher concentrations of RA, and down-regulated more at day 6 than at day 4 (Fig. 2). The result of this study showed that RA also concentration-dependently facilitates terminal differentiation of neural cells derived from ES cells. The expression levels of markers of differentiated neurons and glia, i.e., of βIII-tubulin and GFAP, respectively, was higher in EBs treated with higher concentrations of RA, whereas the expression levels of markers of undifferentiated neural cells, i.e., of Nestin, Group B1 Sox, Olig2, and *sox1* mRNA, was inversely correlated with the concentration of RA (Figs. 2 and 3). The findings are consistent with a high-RA enhancing differentiation of neural progenitor cells, as described previously (Bain et al., 1995, 1996; Fraichard et al., 1995; Gajovic et al., 1997; Renoncourt et al., 1998; Strubing et al., 1995; Wichterle et al., 2002).

Down-regulation of Wnt signaling has been shown to be one of the mechanisms involved in RA-induced neural differentiation of mouse ES cells (Aubert et al., 2002). Interestingly, β-catenin, which is a key molecule in Wnt signaling, has been shown to interact directly with retinoid receptor RAR, but not with RXR, in a retinoid-dependent manner, and as a result retinoids decrease β-catenin-Lef/Tcf-mediated transactivation in cultured cells in a dose-dependent manner (Easwaran et al., 1999). Wnt3a signaling through Lef/Tcf1 has also been implicated in suppression of neural differentiation and induction of mesodermal differentiation in the mouse embryo (Galceran et al., 1999; Yamaguchi et al., 1999; Yoshikawa et al., 1997). These findings raise the possibility that the one of the effects of RA in EBs is to inhibit the Wnt-β-catenin anti-neural pathway by up-regulation of Secreted frizzled-related protein 2 (Sfrp2) (Aubert et al., 2002) and/or sequestration of β-catenin in a concentration-dependent manner, thereby resulting in the promotion of neural differentiation, and inversely in the suppression of mesodermal differentiation.

FGFs are another molecules that may be involved in the neurogenesis related to RA signaling. RA has been shown to promote neuronal differentiation by repressing FGF signalings from the posterior neural plate. Caudal FGF signalings

have the opposite effects and repress Raldh2 (RA synthesis) in the presomatic mesoderm and generic neuronal differentiation in chick early neural tube (Diez del Corral et al., 2003; Novitch et al., 2003). These observations raise the possibility that RA inhibits the action of endogenously generated FGFs in a concentration-dependent manner during the culture of EBs. Further study of the associations between these signals is required to clarify the mechanism underlying the RA-promoted neural differentiation of ES cells.

Acquisition of rostro-caudal identity depends on the concentration of RA

A previous study on chick embryos showed that the default identity of early neural tissue is a rostral location and that neural cells can be caudalized by exogenous factors, such as the caudalizing activity of paraxial mesoderm, FGFs, and retinoid from the mesoderm, which induce midbrain, hindbrain, and spinal cord characters, when applied during the appropriate period of development (Muhr et al., 1999).

RA is one of the factors, that has been shown to be involved in hindbrain patterning and the caudalization of neural tissues in the early embryonic CNS in vivo (Maden, 2002). The distribution of endogenous RA has been examined in mouse and chick embryos, by various method, including HPLC (high-performance liquid chromatography) (Horton and Maden, 1995; Maden et al., 1998), the use of *LacZ* reporter cells (Maden et al., 1998; Wagner et al., 1992), and the use of RARβ_2-*LacZ* transgenic mice (Reynolds et al., 1991; Zimmer, 1992). This distribution of endogenous RA is correlated with the opposing action of the two main enzymes involved in RA-metabolism, RA-synthesizing enzyme, Raldh2, which is most strongly expressed in the paraxial mesoderm adjacent to the rostral spinal cord with the rostral boundary of the presumptive first somite (Berggren et al., 1999), and the catabolizing enzyme, Cyp26a1, which is expressed in anterior neuroepithelium. These spatially distributed enzymes create a rostro-caudal RA concentration gradient in vivo (Abu-Abed et al., 2001; Fujii et al., 1997; Maden et al., 1998; Sakai et al., 2001; Swindell et al., 1999), with the peak RA concentration occurring at the hindbrain/spinal cord boundary, with levels gradually decreasing anterior and posterior to it. Furthermore, it has been suggested that the patterning of the rhombomere is influenced over time by the constant supply of RA from the paraxial mesoderm, where the neuroepithelium grows and moves away form this source of RA. These findings imply that the more posterior rhombomeres that develop later than the more anterior rhombomeres may have been exposed to higher concentration of RA, leading to the expression of more posterior genes (such as posterior *hox* genes), which require a higher concentration of RA for activation in vivo (Maden, 2002). Our findings are consistent with the above-described putative regulatory mechanism of hindbrain/rostral spinal cord positional specification correlated with the RA concentration gradient in vivo in the following manner. The default positional identity of ES-cell-derived neural cells is specified as anteriormost forebrain, which was acquired in the control and Noggin-exposed EBs. EBs treated with low-RA were specified as midbrain to hindbrain, which is generated earlier and require lower concentrations of RA in vivo, whereas EBs treated with high-RA were specified as posterior hindbrain to rostral spinal cord, which is generated later and requires higher concentrations of RA in vivo. In addition, the fact that even the EBs treated with high-RA expressed genes specific to rostral (*hoxc4* to *hoxc6*), but not to caudal spinal cord (*hoxc8* to *hoxc10*) is consistent with the putative gradient of endogenous RA in vivo with a higher concentration in the rostral spinal cord, and the proposed role of RA in rostral spinal cord determination (Liu et al., 2001). Moreover, other factors may be involved in the activation of RA-responsive genes and the specification of positional identity, such as RA binding proteins, including cellular retinoic acid binding protein (CRABP) 1, which limits the access of RA to the nuclear retinoid receptors. The spatiotemporal pattern of expression of CRABP1 suggests that the fine regional control of availability of RA to the nuclear receptors may also play an important role in the organization of the central nervous system and the differentiation of its progenitors in vivo (Leonard et al., 1995; Maden, 2001; Maden et al., 1992; Ruberte et al., 1993). The role of these RA binding proteins in the regulation of in vitro differentiation of ES-cell-derived neural cells should be investigated further in the future.

RA also affects dorso-ventral positional identity

In contrast to the acquisition of rostro-caudal identity, dorso-ventral identity was analyzed in terms of expression of the transcriptional control of the homeodomain (HD) and basic helix-loop-helix (bHLH) proteins. Previous studies have emphasized the role of Shh signaling in establishing the pattern of expression of ventral spinal cord patterning genes (Jessell, 2000). RA has also been reported to contribute to the ventral patterning of the spinal cord; that is, to the induction of ventral interneurons (V0 and V1) by inducing class I genes, including Dbx1, Dbx2, Evx1, Evx2, and En (Pierani et al., 1999), and to the specification of limb level motor neuron subtypes by the expression of Raldh2 in LMC (Sockanathan and Jessell, 1998). Furthermore, recent studies have revealed involvement of RA from the paraxial mesoderm in the timing of neurogenesis and the patterning of the ventral spinal cord regulating the expression of class I and class II genes via inhibition of FGF signals and in combination with Shh signals (Diez del Corral et al., 2003; Novitch et al., 2003). However, the results of our study showed that the concentration of RA to which EBs were exposed was critical for acquisition of dorso-ventral identity by differentiating ES cells, and the concentration dependency showed a bell-

shaped pattern. This was shown by the pattern of the expression of class I and class II genes (Figs. 6A,B), which determines the dorso-ventral progenitor domains of developing hindbrain and spinal cord. EBs exposed to high-RA exhibit mainly dorsal phenotypes, whereas EBs exposed to low-RA exhibit more ventral phenotypes (Figs. 6–8). The expression pattern of *olig2*, higher at day 4 in EBs treated with high-RA and at day 6 in those treated with low-RA, seems to conflict with this finding; however, there are several possible explanations. One is that this alteration of the expression pattern of *olig2* mimics that in vivo according to the stage of development, with expression in most of the undifferentiated neural/glial progenitor cells in the ventral half of the spinal cord occurring around the period of neural tube closure and later being restricted to the motor neuron domain (pMN domain) of the ventral ventricular region, where the progenitors of motor neurons and oligodendrocytes arise sequentially (Lu et al., 2000; Takebayashi et al., 2000; Zhou et al., 2001). Thus, both the cells collected at day 4 from EBs exposed to high-RA and those collected at day 6 from EBs exposed to low-RA may consist of multipotent neural progenitors expressing Olig2. Furthermore, the role of RA in motor neuron development, such as its effect on the expression of bHLH and HD transcription factors, including Olig2, varies with the stage of development, according to a previous study that analyzed chick spinal cord development (Novitch et al., 2003). Similar alteration of the effects of RA may occur in our culture system and be another possible explanation for the sequential expression pattern of *olig2* in EBs exposed to high-RA.

The ventralization of EBs treated with low-RA can be explained by the finding that the active form of Shh-N, which is secreted by the notochord and floor plate of the developing CNS and ventralizes gene expression of neural progenitors in a concentration-dependent manner in vivo (Jessell, 2000), is more highly expressed on day 6 in EBs treated with low-RA (Figs. 7A–C). The hypothesis that the concentration-dependent activity of RA that defines dorso-ventral identity is mediated by Shh-N was confirmed by the result of treatment with the inhibitor of Shh signaling, cyclopamine (Figs. 7D,E and 8) (Chen et al., 2002a,b; Incardona et al., 1998). Cyclopamine abrogated the ventralization activity of low-RA treatment, and addition of exogenous Shh-N more efficiently ventralized differentiating EB-derived cells that had been exposed to both low-RA and high-RA, in a cyclopamine-sensitive manner. The expression level of *bmp4*, which dorsalizes neural progenitor cells (Caspary and Anderson, 2003; Jessell, 2000; Knecht and Bronner-Fraser, 2002), was not very strongly affected by Shh-N or cyclopamine in EBs exposed to either low-RA or high-RA (Fig 7C, data not shown), indicating that BMP signaling is not the major contributor to RA-mediated dorso-ventral specification. Taken together, these findings suggest that Shh-N expressed in EBs exposed to low-RA may be one of the major signals that ventralize neural progenitors and induce expression of class II genes in addition to class I genes, and that the lack of the shh signal in EBs exposed to high-RA may result in expression of only class I genes and a more dorsalized phenotype, which can be ventralized by exogenous Shh-N protein. The results of this study are consistent with a previous report that RA enhances expression of class I genes, but not of class II genes, in developing chick spinal cord (Diez del Corral et al., 2003; Novitch et al., 2003), and that exogenous Shh-N is required in addition to high-RA for efficient generation of motor neurons during EB formation in vitro (Renoncourt et al., 1998; Wichterle et al., 2002). Because EBs exposed to low-RA are mixed populations and contain many mesodermal cells (Fig. 2) (Rohwedel et al., 1999), they may secrete larger amounts of Shh-N than EBs treated with high-RA, which contain smaller proportions of mesodermal cells.

The discrepancy in response to RA between full-length Shh expression and Shh-N expressions detected by Western blotting (Figs. 7A,B) may be another important finding in this study. In contrast to the expression of full-length Shh being observed in EBs treated with RA at concentration 10^{-8} M and above, generation of Shh-N was detected only in EBs exposed to lower concentrations of RA (Figs. 7A,B), indicating the possible existence of RA-dependent machinery controlling Shh-N production by modulating an auto-processing mechanism by the C-terminus of Shh, which processes full-length Shh into the N-terminus active form, or by altering degradation activity of Shh-N.

Use of mutant ES cells for *indian hedgehog (ihh)* and *smoothened (smo)* has shown that hedgehog signaling is also required for neural differentiation of mouse ES cells by RA (Maye et al., 2004). In our study, however, expression of Group B1 Sox and *sox1* mRNA in EBs treated with low- or high-RA and their dissociates were not down-regulated by cyclopamine (Fig. 8, data not shown), indicating that neural differentiation was not inhibited under our culture conditions even in the presence of cyclopamine. There are two possible explanations for this discrepancy. In our experiments, cyclopamine was added on day 2 after the start of ES cells differentiation, whereas in the mutant ES cells in which hedgehog signaling was disrupted it was disrupted at the start of differentiation, raising the possibility that hedgehog signaling may be one of the factors that is required for the initial commitment of neuroectodermal differentiation. The other possibility is that the concentration of cyclopamine used in our study may not have been adequate to completely block hedgehog signaling, and the residual signaling activity may have been sufficient for the transition of ES-cell-derived ectoderm into neuroectoderm, but not for the ventralization of neural cells.

The mechanism underlying these roles of hedgehog signals in differentiation and specification of ES-cell-derived neural cells needs to be elucidated in the future.

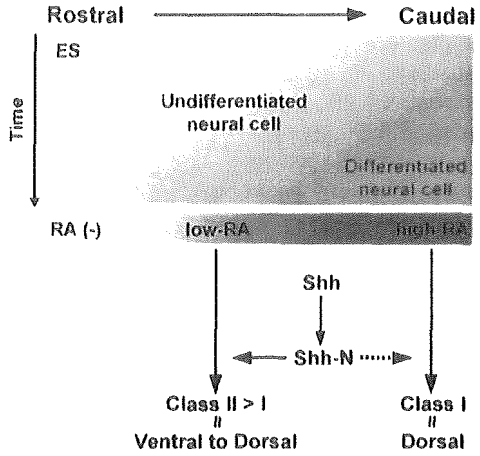

Fig 9. Schematic presentation of the concentration-dependent effects of RA on neural differentiation by mouse ES cells. RA simultaneously promotes both neural differentiation and caudalization in concentration-dependent manner. Low-RA induces a higher level of Shh-N, which endows ES-cell-derived neural progenitors with ventral identity, whereas high-RA poorly induces Shh-N, and they acquire dorsal neural identity instead.

RA is one of the most important inductive signals in vertebrate ontogeny and can be used to induce neural differentiation of mouse ES cells in vitro. However, its actions are complicated and difficult to deal with at will, because RA has the ability to induce various types of cells depending on its concentration, and it simultaneously affects both the timing of differentiation and the acquisition of positional identity, including rostro-caudal and dorso-ventral identity during neural differentiation (Fig. 9). Separation of these two phenomena is desirable to investigate the underlying mechanisms, and separation may have been accomplished, in part, by using SDIA, which is a culture protocol that induces neural cells without RA treatment. Thus, previous studies have shown involvement of RA at a single concentration in the caudalization of ES-cell-derived neural cells (Mizuseki et al., 2003; Wichterle et al., 2002). However, it is still not easy to separate these two phenomena completely during the neural induction of ES cells, because they are simultaneously affected by RA in vivo in combination with other signals, such as FGF and Shh signals, as shown by previous studies (Appel and Eisen, 2003; Diez del Corral et al., 2003; Novitch et al., 2003).

The present study identified detailed gene expression profiles and clarified the effects of the concentration of RA on ES cell differentiation, neuralization, and positional specification, though it may be impossible to map the patterns of expressions of the regional specific markers observed in ES-cell-derived neural cells directly to parallel expression of the markers in vivo. In combination with the RA-independent neural induction method using Noggin, this information will enable us to establish a strategy that will allow control of both the differentiation and the positional identity of neural cells derived from mouse ES cells through EB formation in vitro, and it may be applicable to human ES cells, raising the possibility of application to the treatment of neurological diseases.

Acknowledgments

We are grateful to Dr. H. Niwa for kindly providing ES cell line EB3, Dr. M. Nakafuku for the anti-Olig2 antibody, Dr. J.-F. Brunet for the anti-Phox2b antibody, Dr. O.D. Madsen and Dr. H. Duus for the anti-Nkx6.1 antibody, Dr. H. Kondoh for the anti-GroupB1 Sox antibody, Dr. Y. Takahashi for the xNoggin/BOS plasmid, J. Kohyama, S. Yuasa, and M. Yano for their thoughtful advice, and S. Nakamura for technical assistance. This work was supported by grants from CREST, Japan Society for the Promotion of Science to H.O.

Appendix A. Supplementary data

Supplementary data associated with this article can be found, in the online version, at doi:10.1016/j.ydbio.2004.07.038.

References

Abu-Abed, S., Dolle, P., Metzger, D., Beckett, B., Chambon, P., Petkovich, M., 2001. The retinoic acid-metabolizing enzyme, CYP26A1, is essential for normal hindbrain patterning, vertebral identity, and development of posterior structures. Genes Dev. 15, 226–240.

Acampora, D., Avantaggiato, V., Tuorto, F., Briata, P., Corte, G., Simeone, A., 1998. Visceral endoderm-restricted translation of Otx1 mediates recovery of Otx2 requirements for specification of anterior neural plate and normal gastrulation. Development 125, 5091–5104.

Appel, B., Eisen, J.S., 2003. Retinoids run rampant: multiple roles during spinal cord and motor neuron development. Neuron 40, 461–464.

Arber, S., Han, B., Mendelsohn, M., Smith, M., Jessell, T.M., Sockanathan, S., 1999. Requirement for the homeobox gene Hb9 in the consolidation of motor neuron identity. Neuron 23, 659–674.

Arceci, R., King, A., Simon, M., Orkin, S., Wilson, D., 1993. Mouse GATA-4: a retinoic acid-inducible GATA-binding transcription factor expressed in endodermally derived tissues and heart. Mol. Cell. Biol. 13, 2235–2246.

Aubert, J., Dunstan, H., Chambers, I., Smith, A., 2002. Functional gene screening in embryonic stem cells implicates Wnt antagonism in neural differentiation. Nat. Biotechnol. 20, 1240–1245.

Bain, G., Kitchens, D., Yao, M., Huettner, J.E., Gottlieb, D.I., 1995. Embryonic stem cells express neuronal properties in vitro. Dev. Biol. 168, 342–357.

Bain, G., Ray, W.J., Yao, M., Gottlieb, D.I., 1996. Retinoic acid promotes neural and represses mesodermal gene expression in mouse embryonic stem cells in culture. Biochem. Biophys. Res. Commun. 223, 691–694.

Berggren, K., McCaffery, P., Drager, U., Forehand, C.J., 1999. Differential distribution of retinoic acid synthesis in the chicken embryo as determined by immunolocalization of the retinoic acid synthetic enzyme, RALDH-2. Dev. Biol. 210, 288–304.

Blumberg, B., Bolado Jr., J., Moreno, T.A., Kintner, C., Evans, R.M.,

Papalopulu, N., 1997. An essential role for retinoid signaling in anteroposterior neural patterning. Development 124, 373–379.
Carpenter, E.M., 2002. Hox genes and spinal cord development. Dev. Neurosci. 24, 24–34.
Caspary, T., Anderson, K.V., 2003. Patterning cell types in the dorsal spinal cord: what the mouse mutants say. Nat. Rev., Neurosci. 4, 289–297.
Chen, J.K., Taipale, J., Cooper, M.K., Beachy, P.A., 2002a. Inhibition of Hedgehog signaling by direct binding of cyclopamine to Smoothened. Genes Dev. 16, 2743–2748.
Chen, J.K., Taipale, J., Young, K.E., Maiti, T., Beachy, P.A., 2002b. Small molecule modulation of Smoothened activity. Proc. Natl. Acad. Sci. 99, 14071–14076.
Diez del Corral, R., Olivera-Martinez, I., Goriely, A., Gale, E., Maden, M., Storey, K., 2003. Opposing FGF and retinoid pathways control ventral neural pattern, neuronal differentiation, and segmentation during body axis extension. Neuron 40, 65–79.
Easwaran, V., Pishvaian, M., Salimuddin, S., Byers, S., 1999. Cross-regulation of [beta]-catenin-LEF/TCF and retinoid signaling pathways. Curr. Biol. 9, 1415–1418.
Finley, M.F., Devata, S., Huettner, J.E., 1999. BMP-4 inhibits neural differentiation of murine embryonic stem cells. J. Neurobiol. 40, 271–287.
Fraichard, A., Chassande, O., Bilbaut, G., Dehay, C., Savatier, P., Samarut, J., 1995. in vitro differentiation of embryonic stem cells into glial cells and functional neurons. J. Cell Sci. 108 (Pt 10), 3181–3188.
Fujii, H., Sato, T., Kaneko, S., Gotoh, O., Fujii-Kuriyama, Y., Osawa, K., Kato, S., Hamada, H., 1997. Metabolic inactivation of retinoic acid by a novel P450 differentially expressed in developing mouse embryos. EMBO J. 16, 4163–4173.
Gajovic, S., St-Onge, L., Yokota, Y., Gruss, P., 1997. Retinoic acid mediates Pax6 expression during in vitro differentiation of embryonic stem cells. Differentiation 62, 187–192.
Galceran, J., Farinas, I., Depew, M.J., Clevers, H., Grosschedl, R., 1999. Wnt3a−/− like phenotype and limb deficiency in Lef1−/−Tcf1−/− mice. Genes Dev. 13, 709–717.
Gratsch, T.E., O'Shea, K.S., 2002. Noggin and chordin have distinct activities in promoting lineage commitment of mouse embryonic stem (ES) cells. Dev. Biol. 245, 83–94.
Helms, A.W., Johnson, J.E., 2003. Specification of dorsal spinal cord interneurons. Curr. Opin. Neurobiol. 13, 42–49.
Herrmann, B.G., Labeit, S., Poustka, A., King, T.R., Lehrach, H., 1990. Cloning of the T gene required in mesoderm formation in the mouse. Nature 343, 617–622.
Hitoshi, S., Tropepe, V., Ekker, M., van der Kooy, D., 2002. Neural stem cell lineages are regionally specified, but not committed, within distinct compartments of the developing brain. Development 129, 233–244.
Hooper, M., Hardy, K., Handyside, A., Hunter, S., Monk, M., 1987. HPRT-deficient (Lesch–Nyhan) mouse embryos derived from germline colonization by cultured cells. Nature 326, 292–295.
Horton, C., Maden, M., 1995. Endogenous distribution of retinoids during normal development and teratogenesis in the mouse embryo. Dev. Dyn. 202, 312–323.
Incardona, J., Gaffield, W., Kapur, R., Roelink, H., 1998. The teratogenic Veratrum alkaloid cyclopamine inhibits sonic hedgehog signal transduction. Development 125, 3553–3562.
Jensen, J., Serup, P., Karlsen, C., Nielsen, T.F., Madsen, O.D., 1996. mRNA profiling of rat islet tumors reveals Nkx 6.1as a beta -Cell-specific homeodomain transcription factor. J. Biol. Chem. 271, 18749–18758.
Jessell, T.M., 2000. Neuronal specification in the spinal cord: inductive signals and transcriptional codes. Nat. Rev., Genet. 1, 20–29.
Jonsson, J., Carlsson, L., Edlund, T., Edlund, H., 1994. Insulin-promoter-factor 1 is required for pancreas development in mice. Nature 371, 606–609.
Kawasaki, H., Mizuseki, K., Nishikawa, S., Kaneko, S., Kuwana, Y., Nakanishi, S., Nishikawa, S.I., Sasai, Y., 2000. Induction of midbrain dopaminergic neurons from ES cells by stromal cell-derived inducing activity. Neuron 28, 31–40.
Kawasaki, H., Suemori, H., Mizuseki, K., Watanabe, K., Urano, F., Ichinose, H., Haruta, M., Takahashi, M., Yoshikawa, K., Nishikawa, S., Nakatsuji, N., Sasai, Y., 2002. Generation of dopaminergic neurons and pigmented epithelia from primate ES cells by stromal cell-derived inducing activity. Proc. Natl. Acad. Sci. U. S. A. 99, 1580–1585.
Kessel, M., 1992. Respecification of vertebral identities by retinoic acid. Development 115, 487–501.
Kessel, M., Gruss, P., 1991. Homeotic transformations of murine vertebrae and concomitant alteration of Hox codes induced by retinoic acid. Cell 67, 89–104.
Kim, J.H., Auerbach, J.M., Rodriguez-Gomez, J.A., Velasco, I., Gavin, D., Lumelsky, N., Lee, S.H., Nguyen, J., Sanchez-Pernaute, R., Bankiewicz, K., McKay, R., 2002. Dopamine neurons derived from embryonic stem cells function in an animal model of Parkinson's disease. Nature 418, 50–56.
Knecht, A.K., Bronner-Fraser, M., 2002. Induction of the neural crest: a multigene process. Nat. Rev., Genet. 3, 453–461.
Kohtz, J.D., Lee, H.Y., Gaiano, N., Segal, J., Ng, E., Larson, T., Baker, D.P., Garber, E.A., Williams, K.P., Fishell, G., 2001. N-terminal fatty-acylation of sonic hedgehog enhances the induction of rodent ventral forebrain neurons. Development 128, 2351–2363.
Kohyama, J., Abe, H., Shimazaki, T., Koizumi, A., Okano, H., Hata, J., Umezawa, A., Nakashima, K., Taga, T., Gojo, S., 2001. Brain from bone: Efficient "meta-differentiation" of marrow stroma-derived mature osteoblasts to neurons with Noggin or a demethylating agent. Differentiation 68, 235–244.
Komuro, I., Izumo, S., 1993. Csx: a murine homeobox-containing gene specifically expressed in the developing heart. Proc. Natl. Acad. Sci. 90, 8145–8149.
Lee, S.H., Lumelsky, N., Studer, L., Auerbach, J.M., McKay, R.D., 2000. Efficient generation of midbrain and hindbrain neurons from mouse embryonic stem cells. Nat. Biotechnol. 18, 675–699.
Leonard, L., Horton, C., Maden, M., Pizzey, J.A., 1995. Anteriorization of CRABP-1 expression by retinoic acid in the developing mouse central nervous system and its relationship to teratogenesis. Dev. Biol. 168, 514–528.
Lints, T., Parsons, L., Hartley, L., Lyons, I., Harvey, R., 1993. Nkx-2.5: a novel murine homeobox gene expressed in early heart progenitor cells and their myogenic descendants. Development 119, 419–431.
Liu, J.P., Laufer, E., Jessell, T.M., 2001. Assigning the positional identity of spinal motor neurons: rostrocaudal patterning of Hox-c expression by FGFs, Gdf11, and retinoids. Neuron 32, 997–1012.
Lu, Q.R., Yuk, D.-i., Alberta, J.A., Zhu, Z., Pawlitzky, I., Chan, J., McMahon, A.P., Stiles, C.D., Rowitch, D.H., 2000. Sonic hedgehog-regulated oligodendrocyte lineage genes encoding bHLH proteins in the mammalian central nervous system. Neuron 25, 317–329.
Maden, M., 2001. Role and distribution of retinoic acid during CNS development. Int. Rev. Cytol. 209, 1–77.
Maden, M., 2002. Retinoid signalling in the development of the central nervous system. Nat. Rev., Neurosci. 3, 843–853.
Maden, M., Horton, C., Graham, A., Leonard, L., Pizzey, J., Siegenthaler, G., Lumsden, A., Eriksson, U., 1992. Domains of cellular retinoic acid-binding protein I (CRABP I) expression in the hindbrain and neural crest of the mouse embryo. Mech. Dev. 37, 13–23.
Maden, M., Sonneveld, E., van der Saag, P., Gale, E., 1998. The distribution of endogenous retinoic acid in the chick embryo: implications for developmental mechanisms. Development 125, 4133–4144.
Marquardt, T., Pfaff, S.L., 2001. Cracking the transcriptional code for cell specification in the neural tube. Cell 106, 651–654.
Marshall, H., Nonchev, S., Sham, M.H., Muchamore, I., Lumsden, A., Krumlauf, R., 1992. Retinoic acid alters hindbrain Hox code and induces transformation of rhombomeres 2/3 into a 4/5 identity. Nature 360, 737–741.

Marti, E., Takada, R., Bumcrot, D., Sasaki, H., McMahon, A., 1995. Distribution of Sonic hedgehog peptides in the developing chick and mouse embryo. Development 121, 2537–2547.

Maye, P., Becker, S., Siemen, H., Thorne, J., Byrd, N., Carpentino, J., Grabel, L., 2004. Hedgehog signaling is required for the differentiation of ES cells into neurectoderm. Dev. Biol. 265, 276–290.

McGowan, K.M., Coulombe, P.A., 1998. Onset of keratin 17 expression coincides with the definition of major epithelial lineages during skin development. J. Cell Biol. 143, 469–486.

Mizuguchi, R., Sugimori, M., Takebayashi, H., Kosako, H., Nagao, M., Yoshida, S., Nabeshima, Y., Shimamura, K., Nakafuku, M., 2001. Combinatorial roles of olig2 and neurogenin2 in the coordinated induction of pan-neuronal and subtype-specific properties of motoneurons. Neuron 31, 757–771.

Mizuseki, K., Sakamoto, T., Watanabe, K., Muguruma, K., Ikeya, M., Nishiyama, A., Arakawa, A., Suemori, H., Nakatsuji, N., Kawasaki, H., Murakami, F., Sasai, Y., 2003. Generation of neural crest-derived peripheral neurons and floor plate cells from mouse and primate embryonic stem cells. Proc. Natl. Acad. Sci. U. S. A. 100, 5828–5833.

Muhr, J., Graziano, E., Wilson, S., Jessell, T.M., Edlund, T., 1999. Convergent inductive signals specify midbrain, hindbrain, and spinal cord identity in gastrula stage chick embryos. Neuron 23, 689–702.

Niederreither, K., Vermot, J., Schuhbaur, B., Chambon, P., Dolle, P., 2000. Retinoic acid synthesis and hindbrain patterning in the mouse embryo. Development 127, 75–85.

Niwa, H., Miyazaki, J., Smith, A.G., 2000. Quantitative expression of Oct-3/4 defines differentiation, dedifferentiation or self-renewal of ES cells. Nat. Genet. 24, 372–376.

Novitch, B.G., Chen, A.I., Jessell, T.M., 2001. Coordinate regulation of motor neuron subtype identity and pan-neuronal properties by the bHLH repressor Olig2. Neuron 31, 773–789.

Novitch, B.G., Wichterle, H., Jessell, T.M., Sockanathan, S., 2003. A requirement for retinoic acid-mediated transcriptional activation in ventral neural patterning and motor neuron specification. Neuron 40, 81–95.

Offield, M., Jetton, T., Labosky, P., Ray, M., Stein, R., Magnuson, M., Hogan, B., Wright, C., 1996. PDX-1 is required for pancreatic outgrowth and differentiation of the rostral duodenum. Development 122, 983–995.

Okabe, S., Forsberg-Nilsson, K., Spiro, A.C., Segal, M., McKay, R.D., 1996. Development of neuronal precursor cells and functional postmitotic neurons from embryonic stem cells in vitro. Mech. Dev. 59, 89–102.

Pattyn, A., Morin, X., Cremer, H., Goridis, C., Brunet, J., 1997. Expression and interactions of the two closely related homeobox genes Phox2a and Phox2b during neurogenesis. Development 124, 4065–4075.

Pattyn, A., Hirsch, M., Goridis, C., Brunet, J., 2000. Control of hindbrain motor neuron differentiation by the homeobox gene Phox2b. Development 127, 1349–1358.

Pevny, L.H., Sockanathan, S., Placzek, M., Lovell-Badge, R., 1998. A role for SOX1 in neural determination. Development 125, 1967–1978.

Pierani, A., Brenner-Morton, S., Chiang, C., Jessell, T.M., 1999. A sonic hedgehog-independent, retinoid-activated pathway of neurogenesis in the ventral spinal cord. Cell 97, 903–915.

Porter, J.A., von Kessler, D.P., Ekker, S.C., Young, K.E., Lee, J.J., Moses, K., Beachy, P.A., 1995. The product of hedgehog autoproteolytic cleavage active in local and long-range signalling. Nature 374, 363–366.

Porter, J.A., Ekker, S.C., Park, W.J., von Kessler, D.P., Young, K.E., Chen, C.H., Ma, Y., Woods, A.S., Cotter, R.J., Koonin, E.V., Beachy, P.A., 1996. Hedgehog patterning activity: role of a lipophilic modification mediated by the carboxy-terminal autoprocessing domain. Cell 86, 21–34.

Renoncourt, Y., Carroll, P., Filippi, P., Arce, V., Alonso, S., 1998. Neurons derived in vitro from ES cells express homeoproteins characteristic of motoneurons and interneurons. Mech. Dev. 79, 185–197.

Reynolds, K., Mezey, E., Zimmer, A., 1991. Activity of the beta-retinoic acid receptor promoter in transgenic mice. Mech. Dev. 36, 15–29.

Roelink, H., Porter, J.A., Chiang, C., Tanabe, Y., Chang, D.T., Beachy, P.A., Jessell, T.M., 1995. Floor plate and motor neuron induction by different concentrations of the amino-terminal cleavage product of sonic hedgehog autoproteolysis. Cell 81, 445–455.

Rohwedel, J., Guan, K., Wobus, A.M., 1999. Induction of cellular differentiation by retinoic acid in vitro. Cells Tissues Organs 165, 190–202.

Ross, S.A., McCaffery, P.J., Drager, U.C., De Luca, L.M., 2000. Retinoids in Embryonal Development. Physiol. Rev. 80, 1021–1054.

Ross, S.E., Greenberg, M.E., Stiles, C.D., 2003. Basic helix-loop-helix factors in cortical development. Neuron 39, 13–25.

Ruberte, E., Friederich, V., Chambon, P., Morriss-Kay, G., 1993. Retinoic acid receptors and cellular retinoid binding proteins: III. Their differential transcript distribution during mouse nervous system development. Development 118, 267–282.

Sakai, Y., Meno, C., Fujii, H., Nishino, J., Shiratori, H., Saijoh, Y., Rossant, J., Hamada, H., 2001. The retinoic acid-inactivating enzyme CYP26 is essential for establishing an uneven distribution of retinoic acid along the anterio-posterior axis within the mouse embryo. Genes Dev. 15, 213–225.

Schuurmans, C., Guillemot, F., 2002. Molecular mechanisms underlying cell fate specification in the developing telencephalon. Curr. Opin. Neurobiol. 12, 26–34.

Shimazaki, T., Shingo, T., Weiss, S., 2001. The ciliary neurotrophic factor/leukemia inhibitory factor/gp130 receptor complex operates in the maintenance of mammalian forebrain neural stem cells. J. Neurosci. 21, 7642–7653.

Sive, H.L., Draper, B.W., Harland, R.M., Weintraub, H., 1990. Identification of a retinoic acid-sensitive period during primary axis formation in *Xenopus laevis*. Genes Dev. 4, 932–942.

Smith, W.C., Harland, R.M., 1992. Expression cloning of noggin, a new dorsalizing factor localized to the Spemann organizer in *Xenopus* embryos. Cell 70, 829–840.

Sockanathan, S., Jessell, T.M., 1998. Motor neuron-derived retinoid signaling specifies the subtype identity of spinal motor neurons. Cell 94, 503–514.

Strubing, C., Ahnert-Hilger, G., Shan, J., Wiedenmann, B., Hescheler, J., Wobus, A.M., 1995. Differentiation of pluripotent embryonic stem cells into the neuronal lineage in vitro gives rise to mature inhibitory and excitatory neurons. Mech. Dev. 53, 275–287.

Swindell, E.C., Thaller, C., Sockanathan, S., Petkovich, M., Jessell, T.M., Eichele, G., 1999. Complementary domains of retinoic acid production and degradation in the early chick embryo. Dev. Biol. 216, 282–296.

Takebayashi, H., Yoshida, S., Sugimori, M., Kosako, H., Kominami, R., Nakafuku, M., Nabeshima, Y., 2000. Dynamic expression of basic helix-loop-helix Olig family members: implication of Olig2 in neuron and oligodendrocyte differentiation and identification of a new member, Olig3. Mech. Dev. 99, 143–148.

Temple, S., 2001. The development of neural stem cells. Nature 414, 112–117.

Tonegawa, A., Takahashi, Y., 1998. Somitogenesis controlled by noggin. Dev. Biol. 202, 172–182.

Tropepe, V., Hitoshi, S., Sirard, C., Mak, T.W., Rossant, J., van der Kooy, D., 2001. Direct neural fate specification from embryonic stem cells: a primitive mammalian neural stem cell stage acquired through a default mechanism. Neuron 30, 65–78.

Wagner, M., Han, B., Jessell, T., 1992. Regional differences in retinoid release from embryonic neural tissue detected by an in vitro reporter assay. Development 116, 55–66.

Wang, H.-F., Liu, F.-C., 2001. Developmental restriction of the LIM homeodomain transcription factor Islet-1 expression to cholinergic neurons in the rat striatum. Neuroscience 103, 999–1016.

Wichterle, H., Lieberam, I., Porter, J.A., Jessell, T.M., 2002. Directed differentiation of embryonic stem cells into motor neurons. Cell 110, 385–397.

Wilkinson, D.G., Bhatt, S., Herrmann, B.G., 1990. Expression pattern of the mouse T gene and its role in mesoderm formation. Nature 343, 657–659.

Wood, H.B., Episkopou, V., 1999. Comparative expression of the mouse Sox1, Sox2 and Sox3 genes from pre-gastrulation to early somite stages. Mech. Dev. 86, 197–201.

Wurst, W., Bally-Cuif, L., 2001. Neural plate patterning: upstream and downstream of the isthmic organizer. Nat. Rev. Neurosci. 2, 99–108.

Yamaguchi, T.P., Takada, S., Yoshikawa, Y., Wu, N., McMahon, A.P., 1999. T (Brachyury) is a direct target of Wnt3a during paraxial mesoderm specification. Genes Dev. 13, 3185–3190.

Ying, Q.L., Stavridis, M., Griffiths, D., Li, M., Smith, A., 2003. Conversion of embryonic stem cells into neuroectodermal precursors in adherent monoculture. Nat. Biotechnol. 21, 183–186.

Yoshikawa, Y., Fujimori, T., McMahon, A.P., Takada, S., 1997. Evidence that absence ofWnt-3aSignaling promotes neuralization instead of paraxial mesoderm development in the mouse. Dev. Biol. 183, 234–242.

Zhou, Q., Choi, G., Anderson, D.J., 2001. The bHLH transcription factor Olig2 promotes oligodendrocyte differentiation in collaboration with Nkx2.2. Neuron 31, 791–807.

Zimmer, A., 1992. Induction of a RAR beta 2-lacZ transgene by retinoic acid reflects the neuromeric organization of the central nervous system. Development 116, 977–983.

Zimmerman, L.B., De Jesus-Escobar, J.M., Harland, R.M., 1996. The Spemann organizer signal noggin binds and inactivates bone morphogenetic protein 4. Cell 86, 599–606.

THE JOURNAL OF BIOLOGICAL CHEMISTRY
Vol. 279, No. 49, Issue of December 3, pp. 51376–51385, 2004
Printed in U.S.A.

Physical and Functional Interaction between Dorfin and Valosin-containing Protein That Are Colocalized in Ubiquitylated Inclusions in Neurodegenerative Disorders*

Received for publication, June 15, 2004, and in revised form, August 31, 2004
Published, JBC Papers in Press, September 29, 2004, DOI 10.1074/jbc.M406683200

Shinsuke Ishigaki‡§¶, Nozomi Hishikawa‡, Jun-ichi Niwa‡, Shun-ichiro Iemura‖, Tohru Natsume‖, Seiji Hori, Akira Kakizuka**‡‡, Keiji Tanaka§, and Gen Sobue‡§§**

*From the ‡Department of Neurology, Nagoya University Graduate School of Medicine, Nagoya 466-8500, Japan, the §Department of Molecular Oncology, Tokyo Metropolitan Institute of Medical Science, Tokyo 113-8613, Japan, the ‖National Institute of Advanced Science and Technology, Biological Information Research Center, Tokyo 135-0064, Japan, the **Laboratory of Functional Biology, Kyoto University Graduate School of Biostudies, Kyoto 606-8502, Japan, and ‡‡CREST, Japan Science and Technology Agency, Kawaguchi 332-0012, Japan*

Dorfin, a RING-IBR type ubiquitin ligase (E3), can ubiquitylate mutant superoxide dismutase 1, the causative gene of familial amyotrophic lateral sclerosis (ALS). Dorfin is located in ubiquitylated inclusions (UBIs) in various neurodegenerative disorders, such as ALS and Parkinson's disease (PD). Here we report that Valosin-containing protein (VCP) directly binds to Dorfin and that VCP ATPase activity profoundly contributes to the E3 activity of Dorfin. High through-put analysis using mass spectrometry identified VCP as a candidate of Dorfin-associated protein. Glycerol gradient centrifugation analysis showed that endogenous Dorfin consisted of a 400–600-kDa complex and was co-immunoprecipitated with endogenous VCP. *In vitro* experiments showed that Dorfin interacted directly with VCP through its C-terminal region. These two proteins were colocalized in aggresomes in HEK293 cells and UBIs in the affected neurons of ALS and PD. VCP^{K524A}, a dominant negative form of VCP, reduced the E3 activity of Dorfin against mutant superoxide dismutase 1, whereas it had no effect on the autoubiquitylation of Parkin. Our results indicate that VCPs functionally regulate Dorfin through direct interaction and that their functional interplay may be related to the process of UBI formation in neurodegenerative disorders, such as ALS or PD.

Amyotrophic lateral sclerosis (ALS)[1] is one of the most common neurodegenerative disorders, characterized by selective motor neuron degeneration in the spinal cord, brain stem, and cortex. Two genes, CuZn-superoxide dismutase (SOD1) and amyotrophic lateral sclerosis 2 have been identified as responsible genes for familial forms of ALS. Using mutant SOD1 transgenic mice, the pathogenesis of ALS has been partially uncovered. The proposed mechanisms of the motor neuron degeneration in ALS include oxidative toxicity, glutamate receptor abnormality, ubiquitin proteasome dysfunction, inflammatory and cytokine activation, dysfunction of neurotrophic factors, damage to mitochondria, cytoskeletal abnormalities, and activation of the apoptosis pathway (1, 2).

In a previous study (3), we identified several ALS-associated genes using molecular indexing. Dorfin was identified as one of the up-regulated genes in ALS, which contains a RING-IBR (in between ring finger) domain at its N terminus and mediated ubiquitin ligase (E3) activity (3, 4). Dorfin colocalized with Vimentin at the centrosome after treatment with a proteasome inhibitor in cultured cells (4). Dorfin physically bound and ubiquitylated various SOD1 mutants derived from familial ALS patients and enhanced their degradation, but it had no effect on the stability of wild-type SOD1 (5). Overexpression of Dorfin protected neural cells against the toxic effects of mutant SOD1 and reduced SOD1 inclusions (5).

Recent findings indicate that the ubiquitin-proteasome system is widely involved in the pathogenesis of Parkinson's disease (PD), Alzheimer's disease, polyglutamine disease, and Prion diseases as well as ALS (6). From this point of view, we previously analyzed the pathological features of Dorfin in various neurodegenerative diseases and found that Dorfin was predominantly localized not only in Lewy body (LB)-like inclusions in ALS but also in LBs in PD, dementia with Lewy bodies, and glial cell inclusions in multiple system atrophy (7). These characteristic intracellular inclusions composed of aggregated, ubiquitylated proteins surrounded by disorganized filaments are the histopathological hallmark of aging-related neurodegenerative diseases (8).

A structure called aggresome by Johnston *et al.* (9) is formed when the cell capacity to degrade misfolded proteins is exceeded. The aggresome has been defined as a pericentriolar, membrane-free, cytoplasmic inclusion containing misfolded ubiquitylated protein ensheathed in a cage of intermediate filaments, such as Vimentin (9). The formation of the aggresome mimics that of ubiquitylated inclusions (UBIs) in the affected neurons of various neurodegenerative diseases (10). Combined with the fact that Dorfin was localized in aggresomes in cultured cells and UBIs in ALS and other neurode-

* This work was supported by a grant for a Center of Excellence from the Ministry of Education, Culture, Sports, Science, and Technology of Japan. The costs of publication of this article were defrayed in part by the payment of page charges. This article must therefore be hereby marked "*advertisement*" in accordance with 18 U.S.C. Section 1734 solely to indicate this fact.

¶ Research resident of the Japan Foundation for Aging and Health, Psychiatric and Neurological Diseases, and Mental Health.

§§ To whom correspondence should be addressed: Dept. of Neurology, Nagoya University Graduate School of Medicine, Nagoya 466-8500, Japan. Tel.: 81-52-744-2385; Fax: 81-52-744-2384; E-mail: sobueg@med.nagoya-u.ac.jp.

[1] The abbreviations used are: ALS, amyotrophic lateral sclerosis; E3, ubiquitin ligase; ERAD, endoplasmic reticulum-associated degradation; LB, Lewy body; MS, mass spectrometry; LC-MS/MS, liquid chromatography coupled to electrospray tandem mass spectrometry; PD, Parkinson's disease; SOD1, CuZn-superoxide dismutase; UBI, ubiquitylated inclusions; VCP, valosin-containing protein; FLAG-Parkin, pcDNA3.1/FLAG-Parkin; Ub, ubiquitin; MBP, maltose-binding protein; GST, glutathione *S*-transferase; PBS, phosphate-buffered saline; HA, hemagglutinin; WT, wild type.

generative diseases, these observations suggest that Dorfin may have a significant role in the quality control system in the cell. The present study was designed to obtain further clues for the pathophysiological roles of Dorfin. For this purpose, we screened Dorfin-associated proteins using high performance liquid chromatography coupled to electrospray tandem mass spectrometry (LC-MS/MS). The results showed that Valosin-containing protein (VCP), also called p97 or Cdc48 homologue, obtained from the screening, physically and functionally interacted with Dorfin. Furthermore, both Dorfin and VCP proteins colocalized in aggresomes of the cultured cells and in UBIs in various neurodegenerative diseases.

MATERIALS AND METHODS

Plasmids and Antibodies—pCMV2/FLAG-Dorfin vector (FLAG-Dorfin^{WT}) was prepared by PCR using the appropriate design of PCR primers with restriction sites (ClaI and KpnI). The PCR product was digested and inserted into the ClaI-KpnI site in pCMV2 vector (Sigma). pEGFP-Dorfin (GFP-Dorfin), pCMX-VCP^{Wt} (VCP^{Wt}), and pCMX-VCP^{K524A} (VCP^{K524A}) vectors were described previously (5, 11). pcDNA/HA-VCP^{Wt} (HA-VCP^{Wt}) and pcDNA/HA-VCP^{K524A} (HA-VCP^{K524A}) were subcloned from pCMX-VCP^{Wt} and pCMX-VCP^{K524A}, respectively, into pcDNA3.1 vectors (Invitrogen). The HA tag was introduced at the N terminus of VCP. pcDNA3.1/FLAG-Parkin (FLAG-Parkin) was generated by PCR using the appropriate design of PCR primers with restriction sites (EcoRI and NotI) from pcDNA3.1/Myc-Parkin (12). The FLAG tag was introduced at the N terminus of Parkin. To establish the RING mutant plasmid of Dorfin (FLAG-Dorfin$^{C132S/C135S}$), point mutations for Cys at positions 132 and 135 to Ser were generated by PCR-based site-directed mutagenesis using a QuikChange™ site-directed mutagenesis kit (Stratagene, La Jolla, CA). pcDNA3.1/HA-Ub (HA-Ub), pcDNA3.1/Myc-SOD1^{WT} (SOD1^{WT}-Myc), pcDNA3.1/Myc-SOD1^{G93A} (SOD1^{G93A}-Myc), and pcDNA3.1/Myc-SOD1^{G85R} (SOD1^{G85R}-Myc) were described previously (13, 14). Polyclonal anti-Dorfin (Dorfin-30 and Dorfin-41) and monoclonal anti-VCP antibodies were used as in previous reports (5, 15). The following antibodies were used in this study: monoclonal anti-FLAG antibody (M2; Sigma), monoclonal anti-Myc antibody (9E10; Santa Cruz Biotechnology, Santa Cruz, CA), monoclonal anti-HA antibody (12CA5; Roche Applied Science), polyclonal anti-maltose-binding protein (MBP) antibody (New England BioLabs, Beverly, MA), polyclonal anti-Parkin (Cell Signaling, Beverly, MA), and polyclonal anti-SOD1 (SOD-100; Stressgen, San Diego, CA).

Cell Culture and Transfection—All media and reagents for cell culture were purchased from Invitrogen. HEK293 cells were grown in Dulbecco's modified Eagle's medium containing 10% fetal calf serum, 5 units/ml penicillin, and 50 μg/ml streptomycin. HEK293 cells at subconfluence were transfected with the indicated plasmids using FuGENE6 reagent (Roche Applied Science). To inhibit cellular proteasome activity, cells were treated with 1 μM MG132 (benzyloxycarbonyl-Leu-Leu-Leu-al; Sigma) for 16 h after overnight post-transfection. Cells were analyzed at 24–48 h after transfection.

Protein Identification by LC-MS/MS Analysis—FLAG-Dorfin^{WT} was expressed in HEK293 cells (semiconfluent in a 10-cm dish) and then immunoprecipitated by anti-FLAG antibody. The immunoprecipitates were eluted with a FLAG peptide and then digested with Lys-C endopeptidase (*Achromobacter* protease I). The resulting peptides were analyzed using a nanoscale LC-MS/MS system as described previously (16). The peptide mixture was applied to a Mightysil-PR-18 (1-μm particle, Kanto Chemical Corp., Tokyo) column (45 × 0.150 mm ID) and separated using a 0–40% gradient of acetonitrile containing 0.1% formic acid over 30 min at a flow rate of 50 nl/min. Eluted peptides were sprayed directly into a quadrupole time-of-flight hybrid mass spectrometer (Q-Tof *Ultima*; Micromass, Manchester, UK). MS and MS/MS spectra were obtained in data-dependent mode. Up to four precursor ions above an intensity threshold of 10 cps were selected for MS/MS analysis from each survey scan. All MS/MS spectra were searched against protein sequences of Swiss Prot and RefSeq (NCBI) using batch processes of the Mascot software package (Matrix Science, London, UK). The criteria for match acceptance were the following: 1) when the match score was 10 over each threshold, identification was accepted without further consideration; 2) when the difference of score and threshold was lower than 10 or when proteins were identified based on a single matched MS/MS spectrum, we manually confirmed the raw data prior to acceptance; 3) peptides assigned by less than three y series ions and peptides with +4 charge state were all eliminated regardless of their scores.

Recombinant Proteins and Pull-down Assay—We used pMALp2 (New England BioLabs) and pMALp2T (Factor Xa cleavage site of pMALp2 was replaced with a thrombin recognition site) to express fusion proteins with MBP. To produce the full-length (residues 1–838) Dorfin (MBP-Dorfin^{full}), N-terminal (residues 1–367) Dorfin (MBP-Dorfin^{N}), and C-terminal (residues 368–838) Dorfin (MBP-Dorfin^{C}), the PCR fragments were amplified from pcDNA4/HisMax-Dorfin (4) by using the appropriate PCR primers with restriction sites (FbaI and HindIII) and then ligated into pMAL-p2 vectors. To produce the MBP-Parkin protein, full-length *PARKIN* cDNA was inserted into the EcoRI-NotI sites of pMALp2T. All of the MBP-tagged recombinant proteins were purified from *Escherichia coli* BL21-codon-plus. The detail of the purification method of MBP-tagged proteins was described previously (17). Recombinant GST fusion VCP^{WT} and VCP^{K524A} proteins were also generated from *E. coli* lysate and purified with glutathione-Sepharose. Recombinant His-VCP^{WT} and His-VCP^{K524A} proteins were purified from insect cells using baculovirus. The detail of purification of these recombinant VCP proteins was described previously (15). Binding experiments were performed with proteins carrying different tags. His- or GST-VCP were mixed with MBP fusion proteins: MBP-Dorfin^{full}, -Dorfin^{N}, -Dorfin^{C}, -Parkin, and -mock. His-VCP and GST-VCP proteins were precipitated by Ni^{2+}-nitrilotriacetic acid-agarose (Qiagen, Valencia, CA), and glutathione-Sepharose (Amersham Biosciences), respectively. Binding was performed with 1–3 μg of each protein in 300 μl of binding buffer (50 mM Tris-HCl, pH 7.5, 100 mM NaCl, 5 mM $MgCl_2$, 10% glycerol, 0.5 mg/ml bovine serum albumin, 1 mM dithiothreitol) for 1 h at 4 °C. Then 15 μl of beads were added and incubated for 30 min. The beads were washed by binding buffer three times and eluted with sample buffer and analyzed by SDS-PAGE followed by Western blotting using specific antibodies.

Glycerol Gradient Centrifugation—Cultured cells or mouse tissues were homogenized in 1 ml of PBS with protease inhibitor (Complete Mini; Roche Applied Science). Supernatants (1 mg of protein for cultured cells, 5 mg of protein for mouse tissues, and 0.1 mg of recombinant His-VCP protein) were used as the samples after 10,000 × *g* centrifugation for 20 min. The samples (1.0 ml) were loaded on top of a 34-ml linear gradient of glycerol (10–40%) prepared in 25 mM Tris-HCl buffer, pH 7.5, containing 1 mM dithiothreitol in 40 PA centrifuge tubes (Hitachi, Tokyo), and centrifuged at 4 °C and 80,000 × *g* for 22 h using a Himac CP100α centrifuge system (Hitachi). Thirty fractions were collected from the top of the tubes. Two hundred μl of each fraction was precipitated with acetone, and the remaining pellet was lysed with 50 μl of sample buffer and then used for SDS-PAGE followed by Western blotting.

Immunological Analysis—Cells (4 × 10^5 in a 6-cm dish) were lysed with 500 μl of lysis buffer (50 mM Tris-HCl, 150 mM NaCl, 1% Nonidet P-40, and 1 mM EDTA) with protease inhibitor mixture (Complete Mini) 24–48 h after transfection. The lysate was then centrifuged at 10,000 × *g* for 10 min at 4 °C to remove debris. A 10% volume of the supernatants was used as the "lysate" for SDS-PAGE. When immunoprecipitated, the supernatants were precleared with protein A-Sepharose (Amersham Biosciences), and specific antibodies, anti-FLAG (M2), anti-Myc (9E10), or anti-Dorfin (Dorfin-30) were then added and then incubated at 4 °C with rotation. Immune complexes were then incubated with protein A-Sepharose for 3 h, collected by centrifugation, and washed four times with the lysis buffer. For protein analysis, immune complexes were dissociated by heating in SDS-PAGE sample buffer and loaded onto SDS-PAGE. The samples were separated by SDS-PAGE (12% gel or 4–12% gradient gel) and transferred onto a polyvinylidene difluoride membrane. Finally, Western blotting was performed with specific antibodies.

Immunohistochemistry—HEK293 cells grown on glass coverslips were fixed in 4% paraformaldehyde in PBS for 15 min. Then the cells were blocked for 30 min with 5% (v/v) normal goat serum in PBS, incubated for 1 h at 37 °C with anti-HA antibody (12CA5), washed with PBS, and incubated for 30 min with Alexa 496-nm anti-mouse antibodies (Molecular Probes, Inc., Eugene, OR). The coverslips were washed and mounted on slides. Fluorescence images were obtained using a fluorescence microscope (DMIRE2; Leica, Bannockburn, IL) equipped with a cooled charge-coupled device camera (CTR MIC; Leica). Pictures were taken using Leica Qfluoro software.

Pathological Studies—Pathological studies were carried out on 10% formalin-fixed, paraffin-embedded spinal cords and brain stems filed in the Department of Neurology, Nagoya University Graduate School of Medicine. The specimens were obtained at autopsy from three sporadic cases of ALS and four sporadic PD patients. The spinal cord and brain stem specimens of these ALS and PD cases were immunohistochemically stained with antibodies against Dorfin (Dorfin-41) and VCP. Dou-

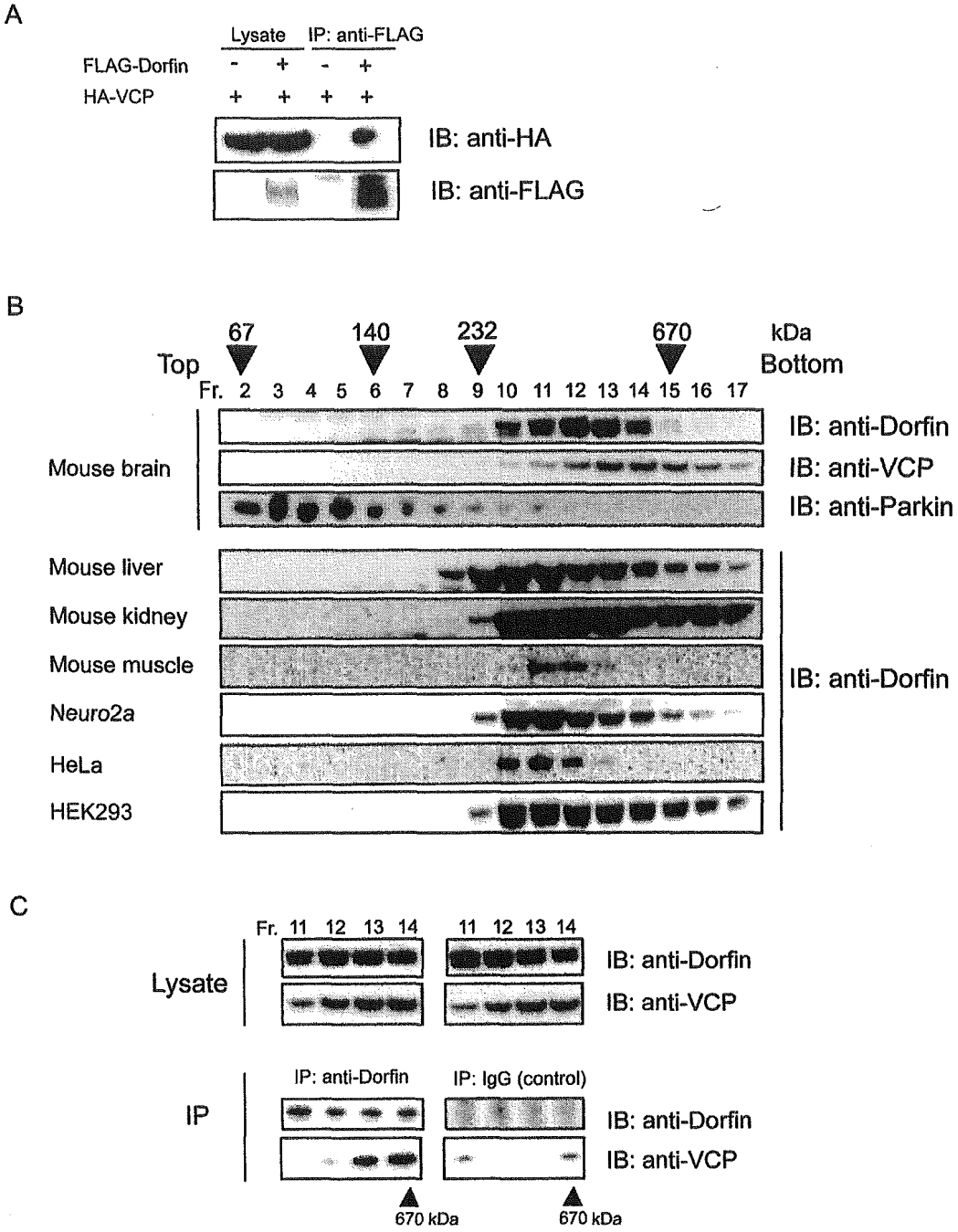

FIG. 1. ***In vivo* interaction between Dorfin and VCP.** *A*, FLAG-Dorfin and HA-VCP are co-expressed in HEK293 cells. FLAG-mock vector was used as a negative control. The amounts of HA-VCP in 10% of the lysate used are shown (*Lysate*); the rest was subjected to immunoprecipitation (*IP*) with anti-FLAG (M2) antibody. Following immunoblotting (*IB*) with anti-HA (12CA5) antibody revealed that HA-VCP was co-immunoprecipitated with FLAG-Dorfin. *B*, 5 mg of protein of various mouse tissues (brain, liver, kidney, and muscle) and 1 mg of protein of cultured cells (HEK293, HeLa, and Neuro2a) were each homogenized in 1 ml of PBS. Supernatants were fractionated by 10–40% glycerol gradient centrifugation followed by separation into 30 fractions using a fraction collector. Immunoblotting using anti-Dorfin, anti-VCP, and anti-Parkin antibodies was performed on the fractions (*Fr.*), including fractions 2–17. Endogenous Dorfin was co-sedimented with VCP in the fractions with a molecular mass of around 400–600 kDa. The positions of co-migrated molecular mass markers are indicated *above* the *panels*. *C*, immunoprecipitation with polyclonal anti-Dorfin antibody (anti-Dorfin-30) was performed on fractions 11–14 collected by glycerol gradient centrifugation analysis, where endogenous Dorfin was seen in *B*. As a negative control, immunoprecipitation with nonimmune rabbit IgG was used on the same fractions.

ble staining of identical sections was performed as described previously (7). In immunofluorescence microscopy, Alexa-488- and Alexa-546-conjugated secondary antibodies (Molecular Probes) were used. All human and animal studies described in this report were approved by the appropriate Ethics Review Committees of the Nagoya University Graduate School of Medicine.

RESULTS

Identification of Dorfin-associated Protein in the Cells—In an effort to identify protein(s) that physically interacts with Dorfin in the cells, FLAG-Dorfin was expressed in HEK293 cells and then immunoprecipitated by anti-FLAG antibody. The immunoprecipitates were eluted with a FLAG peptide and then digested with Lys-C endopeptidase (*Achromobacter* protease I), and the cleaved fragments were directly analyzed using a highly sensitive "direct nanoflow LC-MS/MS" system as described under "Materials and Methods." Following data base search, a total of 13 peptides were assigned to MS/MS spectra obtained from the LC-MS/MS analyses for the FLAG-Dorfin-

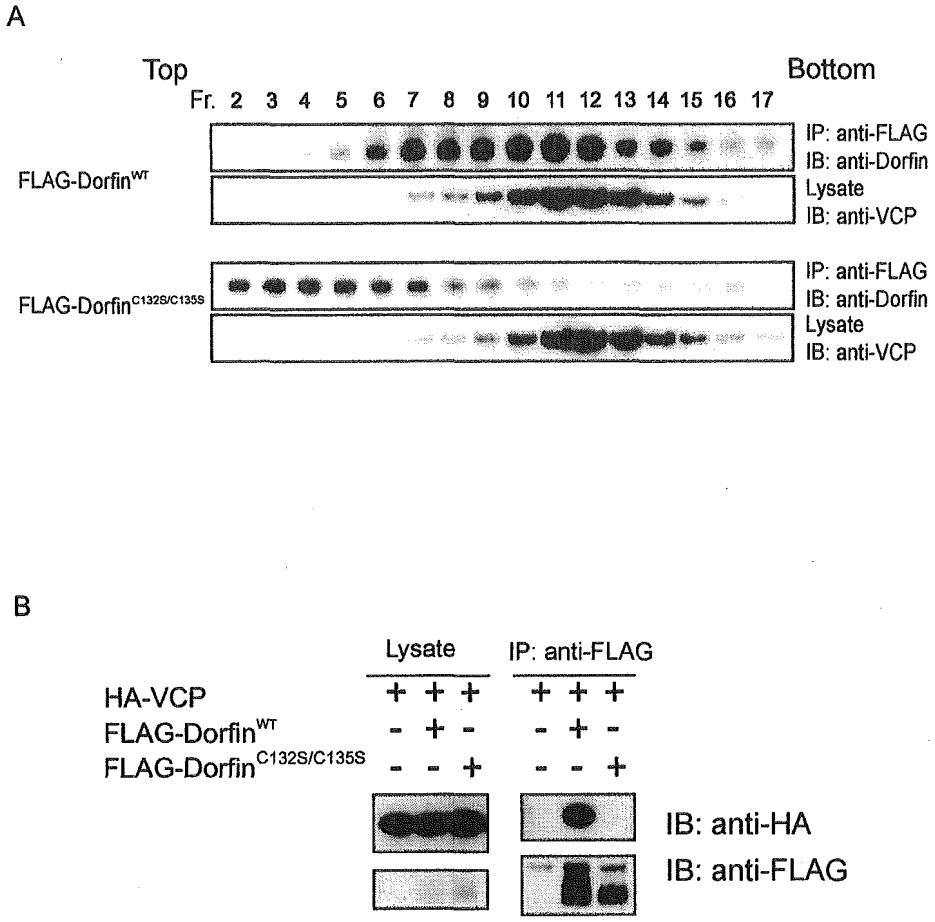

FIG. 2. **Loss of physical interaction between Dorfin$^{C132S/C135S}$ and VCP.** *A*, transfected Dorfin^{WT}, but not Dorfin$^{C132S/C135S}$ (*Dorfin$^{C132S-C135S}$*), forms a high M_r complex. Lysate of HEK293 cells overexpressed with FLAG-Dorfin^{WT} or FLAG-Dorfin$^{C132S/C135S}$ was fractionated by 10–40% glycerol gradient centrifugation. The selected fractions (*Fr.*), fractions 2–17, were subjected to immunoprecipitation (*IP*) using anti-FLAG (M2) antibody. Immunoblotting (*IB*) with anti-Dorfin antibody revealed that exogenous FLAG-Dorfin^{WT} formed a high molecular weight complex, whose peak was at fraction 11, whereas FLAG-Dorfin$^{C132S/C135S}$ migrated in fractions of smaller M_r (around fraction 7). Ten percent of the fractionated samples were shown as "lysate." *B*, Dorfin^{WT} can interact with VCP, but Dorfin$^{C132S/C135S}$ cannot. FLAG-Dorfin^{WT} or FLAG-Dorfin$^{C132S/C135S}$ and HA-VCP were co-expressed in HEK293 cells. FLAG-mock vector was used as a negative control. The amounts of HA-VCP in 10% of the lysate used are shown (*Lysate*); the rest was subjected to immunoprecipitation with anti-FLAG (M2) antibody. Following immunoblotting with anti-HA (12CA5) antibody revealed that HA-VCP was co-immunoprecipitated with FLAG-Dorfin^{WT} but not with FLAG-Dorfin$^{C132S/C135S}$.

associated complexes. These peptide data identified nine proteins as candidates for Dorfin-associated proteins. One of these identified proteins was VCP that has been proposed to have multiple functions, such as membrane fusion or endoplasmic reticulum-associated degradation (ERAD) (18–22). In the next step, we examined the relationship between Dorfin and VCP, because the latter has been reported to be linked to various aspects of neurodegeneration (15).

Dorfin Interacts with VCP in Vivo—To verify the interaction between Dorfin and VCP, FLAG-Dorfin and HA-VCP were transiently overexpressed in HEK 293 cells. Immunological analyses revealed that HA-VCP was co-immunoprecipitated with FLAG-Dorfin but not with FLAG-mock (Fig. 1*A*), confirming their physical interactions in the cells. To determine whether endogenous Dorfin forms a complex, the lysate from mouse brain homogenate was fractioned by glycerol density gradient centrifugation. Each fraction was immunoblotted with anti-Dorfin antibody. The majority of endogenous Dorfin was co-sedimented with VCP around a size of 400–600 kDa, although endogenous Parkin, which is another RING-IBR type E3 ligase (12), existed in the fractions of much lighter molecular weight (M_r) (Fig. 1*B*, *top panels*). Moreover, Dorfin was sedimented in the fractions of 400–600 kDa in other tissues, such as the liver, kidney, and muscle of mouse, and various cultured cells including Neuro2a, HeLa, and HEK293 cells (Fig. 1*B*, *bottom panels*). To determine whether endogenous Dorfin interacts with VCP, immunoprecipitation using polyclonal anti-Dorfin antibody (Dorfin-30) was performed on the fractions shown in Fig. 1*B*, *top panels*. Endogenous VCP was co-immunoprecipitated with endogenous Dorfin in the fractions of high M_r (fractions (*Fr.*) 13 and 14). No apparent band was observed when precipitated with rabbit IgG (Fig. 1*C*).

Mutations of RING Finger Domain of Dorfin Results in Loss of Dorfin-VCP Interactions—Next, we examined whether transfected Dorfin (FLAG-Dorfin^{WT}) and its RING mutant (FLAG-Dorfin$^{C132S/C135S}$), in which the two Cys residues at positions 132 and 135 within the RING finger domain were substituted for Ser residues, form a complex. The results showed overexpression of FLAG-Dorfin^{WT} in high molecular fractions (*Fr.* in Fig. 2), whose peak was between fractions 10 and 12, whereas overexpressed FLAG-Dorfin$^{C132S/C135S}$ did not consist of high molecular weight complex. Overexpression of FLAG-Dorfin^{WT} or FLAG-Dorfin$^{C132S/C135S}$ did not change the sedimentation pattern of VCP (Fig. 2*A*). Furthermore, immunoprecipitation analysis showed that FLAG-Dorfin^{WT}, but not FLAG-Dorfin$^{C132S/C135S}$, could interact with HA-VCP in HEK293 cells (Fig. 2*B*).

Dorfin Interacts with VCP in Vitro—To confirm the direct

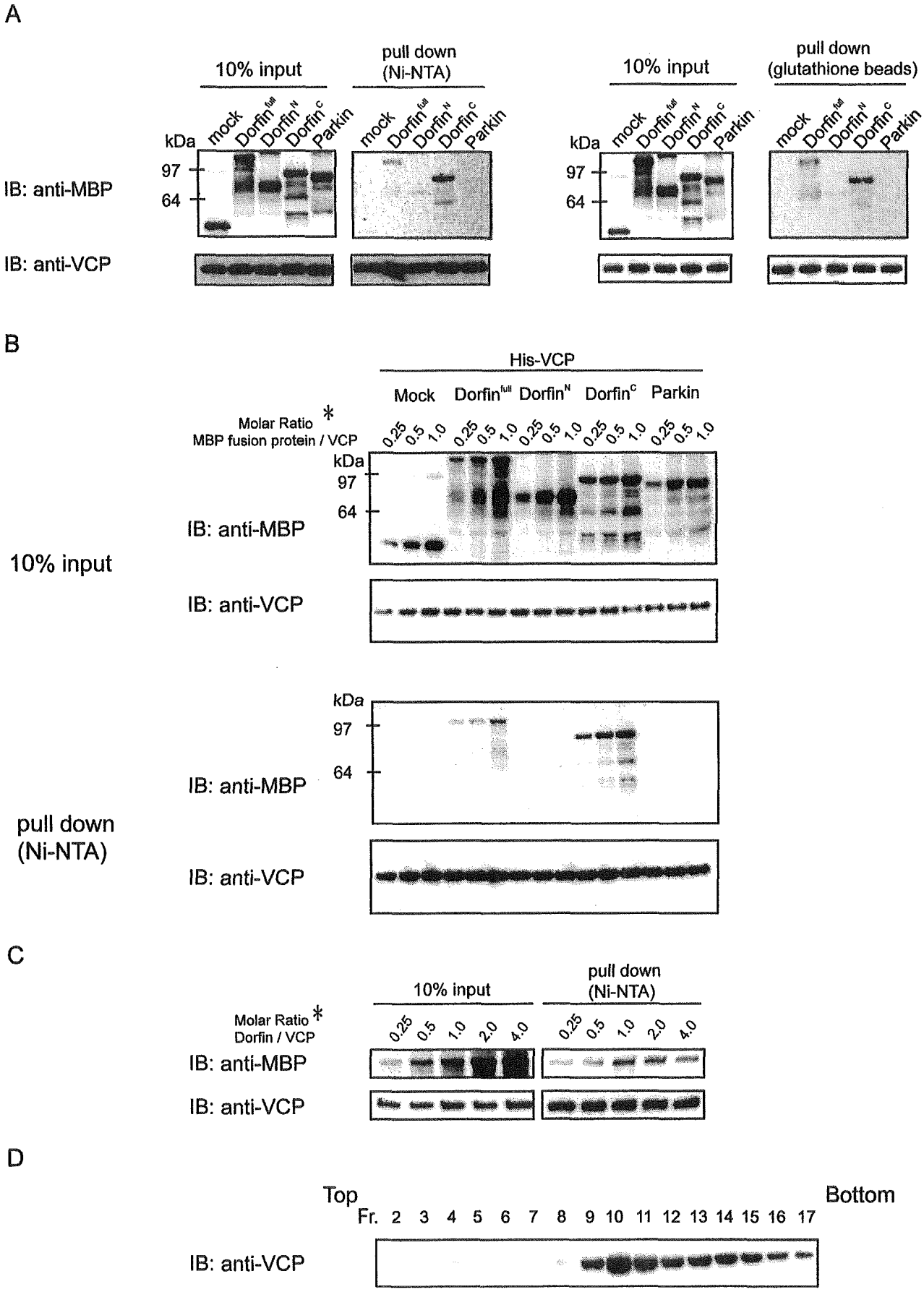

FIG. 3. ***In vitro* interaction between Dorfin and VCP.** *A*, recombinant His- or GST-VCP protein was incubated with MBP-mock, MBP-Dorfin^{full}, MBP-Dorfin^{N}, MBP-Dorfin^{C}, and MBP-Parkin proteins *in vitro*. Two μg of His- or GST-VCP proteins and MBP fusion proteins at similar molar concentrations to VCP proteins were used for the assays. The amounts of MBP fusion and GST fusion Dorfin derivatives and His-VCP in 10% of the samples used are shown (*10% input*). *NTA*, nitrilotriacetic acid. *IB*, immunoblot. *B*, 2 μg of His-VCP was incubated with MBP-mock,

binding between Dorfin and VCP and to determine the exact portion of Dorfin that interacts with VCP *in vitro*, we performed pull-down assays using recombinant proteins. Recombinant MBP-Dorfin or its deletion mutants (*i.e.* MBP-Dorfin^{N} and MBP-Dorfin^{C}) and the same molar of recombinant His-VCP or GST-VCP were mixed and incubated for 1 h at 4 °C. MBP-mock protein was used as a negative control in these experiments. A small portion of MBP-Dorfin^{full} or Dorfin^{C} (C-terminal substrate-recognizing domain) bound to both His-VCP and GST-VCP, whereas MBP-mock, MBP-Dorfin^{N} (N-terminal RING-IBR domain), and MBP-Parkin did not bind to His-VCP or GST-VCP (Fig. 3*A*). We next determined the number of Dorfins that bind one hexamer of VCP. To investigate this issue, we incubated His-VCP with increasing amounts of MBP-Dorfin^{full}, MBP-Dorfin^{N}, MBP-Dorfin^{C}, MBP-mock, or MBP-Parkin. As shown in Fig. 3*B*, the amount of binding portion of MBP-Dorfin^{full} and -Dorfin^{C} pulled down with His-VCP was not saturated below the even molar ratio. The pull-down experiments using excess amounts of MBP-Dorfin^{full} revealed that MBP-Dorfin^{full} was saturated at the even molar ratio (Fig. 3*C*). As reported previously (15), recombinant His-VCP sedimented in high molecular weight fractions, indicating that it formed a hexamer *in vitro* (Fig. 3*D*). These findings indicated that six Dorfin molecules were likely bind to a VCP complex *in vitro*.

Subcellular Localization of Dorfin and VCP in HEK293 Cells—In previous studies, we showed that exogenous and endogenous Dorfin resided perinuclearly and was colocalized with Vimentin in cultured cells treated with a proteasome inhibitor (4). The staining patterns of Dorfin were indistinguishable from those of the aggresome, namely a pericentriolar, membrane-free, cytoplasmic inclusion containing misfolded ubiquitylated proteins packed in a cage of intermediate filaments (4). VCP immunostaining was also observed throughout aggresomes in cultured neuronal cells when induced by treatment with a proteasome inhibitor (15). In order to examine the subcellular localization of Dorfin and VCP, GFP-Dorfin and HA-VCP were co-expressed in HEK293 cells. Without proteasome treatment, GFP-Dorfin-expressing cells showed granular fluorescence in the cytosol, and the HA-VCP-expressing cells showed diffuse and uniform cytoplasmic staining (Fig. 4*A*). Treatment with MG132 (1 μM, 16 h) resulted in accumulation of both GFP-Dorfin and HA-VCP and perinuclear colocalization as a clear large protein aggregate that mimics aggresomes (Fig. 4*B*).

Colocalization of Dorfin and VCP in the Affected Neurons of ALS and PD—In previous studies, immunostaining of Dorfin and VCP was independently noted in LBs of PD, and the peripheral staining pattern of both proteins in LBs was similar (7, 23). To confirm the immunoreactivities of Dorfin and VCP in the affected neurons in ALS and PD, we performed a double-labeling immunofluorescence study using a rabbit polyclonal anti-Dorfin antibody (Dorfin-41) and a mouse monoclonal VCP antibody on the postmortem samples of ALS and PD. In the ALS spinal cords, both proteins were colocalized in the LB-like inclusions (Fig. 5, *A–F*). The margin of LBs in PD was intensely immunostained for Dorfin and VCP, and merged images confirmed their strong colocalization (Fig. 5, *G–L*). Dorfin and VCP were also positive in Lewy neurites in the affected neurons of PD (Fig. 5, *M–O*).

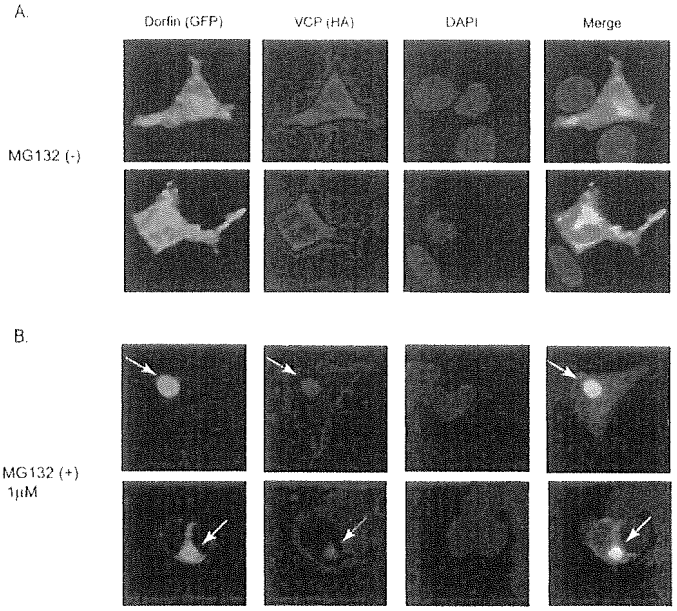

FIG. 4. **Subcellular localization of GFP-Dorfin and HA-VCP in HEK293 cells treated or untreated with a proteasome inhibitor.** GFP-Dorfin and HA-VCP were co-expressed transiently in HEK 293 cells. Cells were treated with (*B*) or without (*A*) 1 μM MG132 for 16 h. HA-VCP was stained with anti-monoclonal HA antibody (12CA5). Nuclei were stained with 4′,6-diamidino-2-phenylindole (*DAPI*). Without the treatment of MG132, GFP-Dorfin was spread through the cytosol, and it appeared like small aggregations. HA-VCP was also seen mainly in the cytosol and partly colocalized with GFP-Dorfin (*A*). After treatment with 1 μM MG132 for 16 h, both GFP-Dorfin and HA-VCP showed perinuclear accumulation and colocalization and appeared as clear large protein aggregates (*B*; *arrows*).

Dorfin Ubiquitylates Mutant SOD1 in Vivo—Unlike the wild-type form, mutant SOD1 proteins are rapidly degraded by the ubiquitin-proteasome system. Consistent with our previous results (5), SOD1^{G93A} and SOD1^{G85R} were polyubiquitylated, and co-expression with FLAG-Dorfin^{WT} enhanced polyubiquitylation of these mutant SOD1s compared with co-expression with FLAG-BAP, a negative control construct (Fig. 6*A*). Boiling with 1% SDS-containing buffer did not change the level of ubiquitylated mutant SOD1, indicating that mutant SOD1 itself was ubiquitylated by Dorfin (Fig. 6*B*). We also performed the same *in vivo* ubiquitylation assay using Neuro2a cells to examine for E3 activity of Dorfin in neuronal cells. The enhanced polyubiquitylation of these mutant SOD1s by Dorfin was observed in Neuro2a cells as well as in HEK293 cells (Fig. 6*C*). FLAG-Dorfin$^{C132S/C135S}$ did not enhance polyubiquitylation of mutant SOD1s, indicating that this RING finger mutant form was functionally inactive (Fig. 6*D*).

VCP^{K524A} Suppresses the E3 Activity of Dorfin—VCP has two ATPase binding domains (D1 and D2). A D2 domain mutant, VCP^{K524A}, induces cytoplasmic vacuoles, which mimics vacuole formation seen in the affected neurons in various neurodegenerative diseases (11, 15). The D2 domain represents the major ATPase activity and is essential for VCP function (11). The ATPase activity of VCP^{K524A} is much lower than that of VCP^{WT}, and VCP^{K524A} caused accumulation of polyubiquitylated proteins in the nuclear and membrane fractions together with elevation of ER stress marker proteins due to ERAD

MBP-Dorfin^{full}, MBP-Dorfin^{N}, MBP-Dorfin^{C}, and MBP-Parkin with increasing amounts (molar ratio to VCP: 0.25, 0.5, and 1.0). The amounts of MBP fusion Dorfin derivatives and His-VCP in 10% of the samples used are shown (10% input). *C*, 2 μg of His-VCP was incubated with MBP-Dorfin^{full} with increasing amounts (molar ratio to VCP: 0.25, 0.5, 1, 2, and 4). The amounts of MBP-Dorfin^{full} and His-VCP in 10% of the samples used are shown (*10% input*). *D*, His-VCP protein (0.5 μg) was fractionated by 10–40% glycerol gradient centrifugation followed by separation into 30 fractions using a fraction collector. Immunoblotting using anti-VCP antibody was performed on the selected fractions (fractions 2–17). *, The molar ratio was calculated by the amount of VCP monomers, not VCP complexes.